One-electron matrix elements in the theory of ion–metal-surface scattering

Uwe Wille
Bereich Schwerionenphysik, Hahn-Meitner-Institut Berlin, Postfach 390128, D-1000 Berlin 39, Germany
(Received 14 October 1991)

A systematic evaluation of one-electron matrix elements appearing in the theory of charge-exchange processes in ion–metal-surface scattering is presented. The conduction-band electrons are described by jellium-type wave functions, while hydrogenic wave functions are employed for the electronic states of the ion. By applying Fourier-transform methods and complex integration techniques, exact closed-form expressions for overlap and Coulomb matrix elements are derived for arbitrary hydrogenic quantum numbers, momenta of the conduction-band electrons, and distances of the ion from the surface. The general case of arbitrary energy difference between initial and final state (including the strictly resonant case) is treated. For the near-resonant case, an expansion of the matrix elements about the resonant limit is derived. The effect of the motion of the ion is taken into account by including electronic translational factors. The actual computation of the matrix elements involves multiple summations, which can be accurately performed even for high-lying ionic Rydberg states. Structural properties of the matrix elements are revealed by studying, for typical cases, their dependence on the various parameters. Possible applications of our method are indicated.

PACS number(s): 79.20.Rf, 79.80.+w

I. INTRODUCTION

For many decades, considerable interest has been devoted to the study of the electronic processes that take place when atoms or ions are scattered by metal surfaces. Following the early investigations on recombination of ions [1–4], the systematic exploration of the basic charge-exchange and electron-emission processes near metal surfaces was initiated by Hagstrum [5]. The development of the field of ion–metal-surface scattering (the term "ion" is understood here and in the following to include the limiting case of a neutral atom) and its present status have been summarized in a number of comprehensive review articles [6–21].

Electronic processes in ion–metal-surface scattering are frequently studied under *near-adiabatic* conditions, under which the energy transfer between the translational motion of the ion and the electronic degrees of freedom in the ion-metal system is small. In this case, one may distinguish essentially two different categories of electronic transitions. First, the *one-electron* potential acting in the ion-metal system can effect *resonant* transitions in which electrons are transferred from occupied states of the conduction band of the metal into empty ionic states having the same energy ("resonance neutralization"), or from loosely bound, occupied ionic states into empty conduction-band states of the same energy ("resonance ionization"). Second, Auger-type *two-electron* transitions can be induced by the electron-electron interaction. In these transitions, a conduction-band electron is transferred into a low-lying, empty ionic core state, with the excess energy being carried away by an electron emitted simultaneously from the conduction band ("Auger neutralization") or from an excited ionic state ("Auger deexcitation").

From a theoretical point of view, the ion-metal interaction constitutes a many-electron problem of extreme complexity. The complete solution of this problem requires the dynamical treatment of one-electron and two-electron processes including effects of the response of the metal electron gas to the presence of the ion ("image charge effects") and effects of the Pauli principle. It is therefore not surprising that a fully quantitative theoretical understanding of ion–metal-surface scattering has not yet been achieved.

Most of the theoretical studies performed so far have treated the ion-metal interaction in the strictly adiabatic limit ("fixed-ion approximation"), using first-order perturbation theory to calculate transition rates for resonant one-electron processes and Auger processes as a function of the ion-surface distance [1–4,22–29,19]. In a number of cases [30–35], nonperturbative approximations at different levels of sophistication have been used to evaluate transition rates in the adiabatic limit. Departures from adiabaticity due to the motion of the ion relative to the surface have been treated within various time-dependent quantal approximation schemes [23,36–45] as well as within a classical master-equation approach [46,40].

While in the past the emphasis has been on studies with light ions in low charge states, the recent development in the field of ion–metal-surface scattering is characterized by an increasing number of experimental investigations using beams of slow, *highly charged, heavy* ions [47,28,48–53]. The advent of this type of experiment constitutes a challenge to theory. In typical scattering experiments with highly charged, heavy ions, the electrons at the Fermi level of the conduction band are near degenerate with high-lying Rydberg states of the incoming ion, so that resonant one-electron transitions into these states will be the dominant charge-exchange process at least at an early stage of the interaction. A sys-

tematic extension of the previously developed theoretical schemes to the regime of ionic Rydberg states is therefore desirable. In recent theoretical studies [54,55] of the interation of highly charged ions with metal surfaces, the classical aspects of electron-transfer processes involving high-lying ionic states have been emphasized. The present paper aims at taking a step towards a fully quantal treatment of the electronic degrees of freedom in these processes.

We consider in this work one-electron *overlap* matrix elements and *Coulomb* matrix elements as they appear in the quantal theory of charge-exchange processes in ion–metal-surface scattering. These matrix elements form the basic ingredients of any specific formulation of the theory [22,20], and their accurate evaluation is prerequisite to the complete analysis of present-day experiments. Our aim is to devise and implement a systematic method for explicitly evaluating the matrix elements for arbitrary values of their parameters, in particular at high principal quantum numbers of the ionic states. We do not impose restrictions on the energies of the initial and final states; i.e., we deal with the case of strict energy resonance as well as with the off-resonance case, which is relevant for treating nonadiabatic effects. Further, we wish to study structural properties of the matrix elements, such as their dependence on the various parameters, without making reference to specific theoretical approximation schemes. We use jellium-type wave functions to describe the metal electrons, whereas hydrogenic wave functions are used for the ionic states.

In the context of previous theoretical studies, matrix elements of the type considered here have been evaluated by different methods for various specific cases, yet exclusively for low values of the ionic quantum numbers (with the exception of Refs. [28,19] in which matrix elements for ionic Rydberg states were evaluated at asymptotically large ion-surface distance) and usually with restrictions imposed on the values of the other parameters. A partially implicit, closed-form representation of one-electron Coulomb matrix elements for arbitrary parameter values has been given in Ref. [41], which has been obtained [56] by employing parametric-differentiation techniques and integration in cylindrical coordinates. No attempt has been made to examine the general applicability of this representation.

The organization of the present paper is as follows. In Sec. II we specify the general form of the matrix elements and perform a reduction to one-dimensional integrals. The key quantities appearing in these integrals are functions $F_j(q_z)$ related to the momentum-space representation $\tilde{\psi}^{(Z)}_{nlm}(\mathbf{q})$ of the ionic wave function $\psi^{(Z)}_{nlm}(\mathbf{r})$. In order to apply complex integration techniques, the analytic structure of the functions $F_j(q_z)$ in the complex q_z plane is explored in Sec. III. In Sec. IV the final evaluation of the matrix elements is performed, and compact closed-form expressions for various specific cases are collected. The efficiency and accuracy of the numerical summation of these expressions is examined. In Sec. V typical examples are explicitly considered, and qualitative structural properties of the matrix elements are derived from these examples. In Sec. VI we summarize the contents of the paper and indicate possible applications of our results. A variety of lengthy formulas is collected in the Appendix. We use atomic units unless stated otherwise.

II. GENERAL FORM AND REDUCTION OF MATRIX ELEMENTS

The physical situation that we consider is depicted schematically in Fig. 1. An ion is located at a fixed, but arbitrary distance D in front of an ideal metal surface. In a laboratory frame with coordinates (x,y,z), the surface is assumed to coincide with the (x,y) plane in such a way that the metal fills the half-space $z \leq 0$. As the metal is invariant with respect to translations in the (x,y) plane, we may assume, without loss of generality, that the ion lies on the z axis, i.e., the coordinates of its center are $(0,0,D)$. An overall phase factor that arises in the matrix elements when the position of the ion is shifted away from the z axis will be included in the final results. The electronic position vector $\mathbf{r}'$ referred to a coordinate frame with origin in the center of the ion is related to the position vector $\mathbf{r}$ referred to the laboratory frame by

$$\mathbf{r}' = \mathbf{r} - D\hat{\mathbf{e}}_z \ , \tag{1}$$

where $\hat{\mathbf{e}}_z$ is the unit vector in the z direction.

The complete one-electron Hamiltonian describing the electronic motion in the ion-metal system [22] comprises the potentials of the unperturbed conduction band and of the ion core as well as the image potentials induced by the ion core and the valence electrons. For our purposes, it is sufficient to write down the Hamiltonian in the form

$$H = -\tfrac{1}{2}\nabla^2 + V_m + V_c \ , \tag{2}$$

in which the image potentials are neglected. The conduction-band potential V_m is taken in the jellium approximation [3,23],

$$V_m = -V_0\Theta(-z) \ , \tag{3}$$

where $V_0 > 0$ is the sum of the Fermi energy ε_F (reckoned from the bottom of the conduction band) and the work function Φ, and $\Theta(z)$ is the unit step function. The Coulomb potential V_c of the ion core is written as

$$V_c = -\frac{Z}{r'}\Theta(z) \equiv -\frac{Z}{|\mathbf{r} - D\hat{\mathbf{e}}_z|}\Theta(z) \ , \tag{4}$$

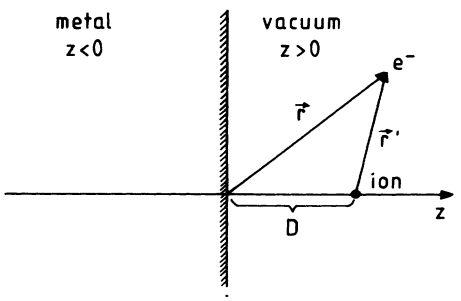

FIG. 1. Schematic diagram showing the choice of coordinates used to describe the ion–metal-surface interaction.

where Z is the effective core charge. The "cutoff" factor $\Theta(z)$ reflects the assumption that inside the metal the ionic potential is completely "screened out" by the polarization charges piled up at the surface.

A. General form of matrix elements

The one-electron matrix elements considered here are of the general form

$$\mathcal{M}_j(\mathbf{k};n,l,m;\mathbf{v},D)=\langle\phi_{\mathbf{k}}^{(V_0)}|f_j^{(\mathbf{v},D)}\rangle \equiv\int d\mathbf{r}[\phi_{\mathbf{k}}^{(V_0)}(\mathbf{r})]^* f_j^{(\mathbf{v},D)}(\mathbf{r}) , \quad (5)$$

where the wave function $\phi_{\mathbf{k}}^{(V_0)}(\mathbf{r})$ is a solution of the one-electron Hamiltonian with the jellium potential (3). Its explicit form will be given in Sec. II B. The function $f_j^{(\mathbf{v},D)}(\mathbf{r})$ is defined as

$$f_j^{(\mathbf{v},D)}(\mathbf{r})=f_j(\mathbf{r}-D\hat{\mathbf{e}}_z)\exp(i\mathbf{v}\cdot\mathbf{r}) \equiv f_j(\mathbf{r}')\exp(i\mathbf{v}\cdot\mathbf{r}) . \quad (6)$$

The subscript j distinguishes the two choices

$$f_1(\mathbf{r}')=\psi_{nlm}^{(Z)}(\mathbf{r}') \quad (7)$$

and

$$f_2(\mathbf{r}')=-\frac{Z}{r'}\psi_{nlm}^{(Z)}(\mathbf{r}') . \quad (8)$$

The function f_1 is an (unperturbed) ion-centered hydrogenic wave function corresponding to effective core charge Z and energy

$$\varepsilon_n=-\frac{1}{2}\frac{Z^2}{n^2} . \quad (9)$$

The resulting matrix element (5) is the overlap matrix element expressing the nonorthogonality of hydrogenic and metal wave functions [22]. In the function f_2, the ion-centered hydrogenic wave function is multiplied by the potential energy of an electron in the Coulomb field of the ion core. The matrix element resulting from inserting the function f_2 into Eq. (5) is commonly [22] assumed to constitute the basic one-electron transition matrix element describing charge exchange processes in ion–metal-surface scattering.

We have included in the function $f_j^{(\mathbf{v},D)}(\mathbf{r})$ a plane-wave translational factor $\exp(i\mathbf{v}\cdot\mathbf{r})$, which serves to impart to an electron bound to the ion, in addition to its internal momentum and energy, a momentum $\mathbf{v}$ and a kinetic energy $\mathbf{v}^2/2$ when the ion moves with velocity $\mathbf{v}$ in the laboratory system. The functions $\psi_{nlm}^{(Z)}(\mathbf{r}')\exp(i\mathbf{v}\cdot\mathbf{r})$ fulfill the asymptotic conditions required for ionic basis functions in a truly *dynamical* treatment of scattering problems [57].

It should be noted here that the hydrogenic wave functions introduced in Eq. (7) are not eigenfunctions of the one-electron Hamiltonian with the "cutoff" core potential given by Eq. (4). The use of functions of the latter type as unperturbed basis functions may be attractive on physical grounds, but their explicit calculation is likely to be prohibitively complicated.

We further mention that we automatically obtain those matrix elements in which the full Coulomb potential is replaced with the cutoff potential (4). In the evaluation of the matrix elements (5), the contributions from inside and outside of the metal emerge from separate calculations. So the contribution to the matrix element with the full Coulomb potential from outside of the metal just gives the total matrix element with the perturbing potential (4). The matrix elements of the metal potential V_m are obtained in a trivial way by multiplying the contribution to the overlap matrix element from inside the metal by a factor $-V_0$.

B. Jellium wave functions

For later use, we have to specify the jellium wave functions in detail and discuss some of their properties. The bound-state jellium wave functions are eigenfunctions of the Hamiltonian

$$H=-\tfrac{1}{2}\nabla^2+V_m\equiv-\tfrac{1}{2}\nabla^2-V_0\Theta(-z) . \quad (10)$$

The wave function corresponding to electronic momentum $\mathbf{k}=(k_x,k_y,k_z)$ [we refer to the parameter k_z as the z component of the electronic momentum although the Hamiltonian (10) does not commute with the z component of the momentum operator] and energy

$$\varepsilon_k=\frac{k^2}{2}-V_0<0 \quad (11)$$

($k=|\mathbf{k}|$) is given [3,23] explicitly by

$$\phi_{\mathbf{k}}^{(V_0)}(\mathbf{r})=\exp(ik_x x)\exp(ik_y y)g_{k_z}^{(V_0)}(z) , \quad (12)$$

where

$$g_{k_z}^{(V_0)}(z)=[\exp(ik_z z)+a\exp(-ik_z z)]\Theta(-z) +b\exp(-\kappa_z z)\Theta(z) . \quad (13)$$

The real quantity κ_z characterizing the decrease of the wave function outside of the metal is expressed in terms of V_0 and k_z as

$$\kappa_z=(2V_0-k_z^2)^{1/2}>0 , \quad (14)$$

so that the energy ε_k can be written as

$$\varepsilon_k=\tfrac{1}{2}(k_\parallel^2-\kappa_z^2) , \quad (15)$$

where

$$k_\parallel=(k_x^2+k_y^2)^{1/2} \quad (16)$$

is the momentum component parallel to the surface.

The reflection and penetration coefficients a and b in Eq. (13) are given by

$$a=\frac{k_z-i\kappa_z}{k_z+i\kappa_z}\equiv\frac{k_z^2-\kappa_z^2}{2V_0}-i\frac{k_z\kappa_z}{V_0}, \quad |a|=1 \quad (17)$$

and

$$b=\frac{2k_z}{k_z+i\kappa_z}\equiv\frac{k_z^2}{V_0}-i\frac{k_z\kappa_z}{V_0}\equiv 1+a , \quad (18)$$

respectively.

Now, by expressing the reflection coefficient a as

$$a=\exp(2i\chi_a)\ , \tag{19}$$

we can rewrite the function $g_{k_z}^{(V_0)}(z)$ for $z<0$ as

$$g_{k_z}^{(V_0)}(z)=\exp(ik_z z)+a\exp(-ik_z z)$$
$$\equiv 2\exp(i\chi_a)\cos(k_z z-\chi_a)\ . \tag{20}$$

The complex phase of $g_{k_z}^{(V_0)}(z)$ in the range $z<0$ is therefore given by χ_a or $\chi_a\pm\pi$, depending on whether $\cos(k_z z-\chi_a)$ is positive or negative. The phase of $g_{k_z}^{(V_0)}(z)$ in the range $z>0$ is given by the phase of the penetration coefficient $b=|b|\exp(i\phi_b)$,

$$\phi_b=-\arctan\left[\frac{\kappa_z}{k_z}\right]\ . \tag{21}$$

It follows from the continuity of $g_{k_z}^{(V_0)}(z)$ at $z=0$ that

$$\chi_a=\phi_b\ . \tag{22}$$

This shows that the *relative* phase between the value of the function $g_{k_z}^{(V_0)}(z)$ at any point in the range $z<0$ and its value at any point in the range $z>0$ can acquire only the values 0 or $\pm\pi$. We will make use of this statement below in order to infer phase relations between the contributions to the matrix elements arising from the half-space $z<0$ and from the half-space $z>0$, respectively.

Another relation which we will have to use below is

$$[\phi_{\mathbf{k}}^{(V_0)}(\mathbf{r})]^*=\phi_{-\mathbf{k}}^{(V_0)}(\mathbf{r})\ . \tag{23}$$

This follows from Eqs. (12), (13), (17), and (18).

Since we deal in this paper with matrix elements only and not with absolute transition rates, we have chosen an arbitrary normalization for the functions $\phi_{\mathbf{k}}^{(V_0)}(\mathbf{r})$. We assume infinite extension of the jellium wave functions, which results in Dirac δ functions when the plane-wave parts are integrated over full space.

C. Reduction to one-dimensional integrals

We now proceed with the evaluation of the matrix element $\mathcal{M}_j(\mathbf{k};n,l,m;\mathbf{v},D)$ by reducing it to a sum of one-dimensional integrals. This is achieved by expressing the function $f_j^{(\mathbf{v},D)}(\mathbf{r})$ in Eq. (5) in terms of the Fourier transform $\tilde{f}_j(\mathbf{q})$ of the function $f_j(\mathbf{r})$. Using Eq. (A2) we obtain

$$f_j^{(\mathbf{v},D)}(\mathbf{r})=(2\pi)^{-3/2}\int d\mathbf{q}\exp[i(\mathbf{q}+\mathbf{v})\cdot\mathbf{r}-iDq_z]$$
$$\times\tilde{f}_j(\mathbf{q})\ . \tag{24}$$

Upon inserting this expression into Eq. (5) and interchanging the order of the integrations over $\mathbf{r}$ and $\mathbf{q}$, we can integrate out the plane-wave factors in the coordinates x and y and use the resulting Dirac δ functions $\delta(q_x-k_x+v_x)$ and $\delta(q_y-k_y+v_y)$ to perform the q_x and q_y integrations. As an intermediate step in the evaluation of the matrix element (5), we then obtain

$$\mathcal{M}_j(\mathbf{k};n,l,m;\mathbf{v},D)=(2\pi)^{1/2}\int_{-\infty}^{+\infty}dq_z F_j(q_z)\exp(-iDq_z)\int_{-\infty}^{+\infty}dz[g_{k_z}^{(V_0)}(z)]^*\exp[i(q_z+v_z)z]\ , \tag{25}$$

where the function $F_j(q_z)$ is defined by

$$F_j(q_z)=\tilde{f}_j(k_x',k_y',q_z)\ , \tag{26}$$

and

$$k_x'=k_x-v_x,\quad k_y'=k_y-v_y \tag{27}$$

are the x and y components, respectively, of the momentum of the metal electron relative to the *moving* ion.

Further, upon inserting the function $g_{k_z}^{(V_0)}(z)$ from Eq. (13) into the z integral of Eq. (25), we encounter integrals of the form

$$I^{\pm}(q_z)=\int_{-\infty}^{0}dz\exp[i(q_z-p^{\pm})z] \tag{28}$$

and

$$I^{>}(q_z)=\int_{0}^{+\infty}dz\exp[i(q_z-p^{>})z]\ , \tag{29}$$

where

$$p^{\pm}=\pm k_z-v_z \tag{30}$$

and

$$p^{>}=-v_z-i\kappa_z\ . \tag{31}$$

The integrals $I^{\pm}(q_z)$ correspond to the range $z<0$, i.e., to the contribution to the matrix element from *inside* the metal. The superscripts "+" and "−" distinguish the contributions arising from the "*incoming*" wave $\exp(ik_z z)$ in $g_{k_z}^{(V_0)}(z)$ and from the *reflected* wave $\exp(-ik_z z)$, respectively. The integral $I^{>}(q_z)$ corresponds to the range $z>0$, i.e., to the contribution to the matrix element from *outside* of the metal.

The integrals $I^{\pm}$ can be carried out after introducing into the exponential an infinitesimally small quantity $i\eta$ where $\eta>0$, in a way that corresponds to a wave function that is exponentially damped for $z\to-\infty$:

$$I^{\pm}(q_z)=\int_{-\infty}^{0}dz\exp[i(q_z-p^{\pm}-i\eta)z]$$
$$=\frac{-i}{q_z-p^{\pm}-i\eta}\ . \tag{32}$$

The limit $\eta\to 0$ is to be performed after the q_z integration in Eq. (25) has been carried out. The integral $I^{>}$ is well defined since $\kappa_z>0$ and therefore $\mathrm{Im}\,p^{>}<0$,

$$I^{>}(q_z)=\frac{i}{q_z-p^{>}}\ . \tag{33}$$

We now introduce integrals $K_j^{\pm}$ and $K_j^{>}$ by setting

$$K_j^{\pm}=\int_{-\infty}^{+\infty}dq_z J_j^{\pm}(q_z) \tag{34}$$

and

$$K_j^{>}=\int_{-\infty}^{+\infty}dq_z J_j^{>}(q_z)\ , \tag{35}$$

where the functions $J_j^{\pm}(q_z)$ and $J_j^{>}(q_z)$ are defined as

$$\begin{aligned}J_j^{\pm}(q_z)&=F_j(q_z)\exp(-iDq_z)I^{\pm}(q_z)\\&\equiv -iF_j(q_z)\frac{\exp(-iDq_z)}{q_z-p^{\pm}-i\eta}\end{aligned} \tag{36}$$

and

$$\begin{aligned}J_j^{>}(q_z)&=F_j(q_z)\exp(-iDq_z)I^{>}(q_z)\\&\equiv iF_j(q_z)\frac{\exp(-iDq_z)}{q_z-p^{>}}\ .\end{aligned} \tag{37}$$

In terms of $K_j^{\pm}$ and $K_j^{>}$, the matrix element (25) is expressed as

$$\begin{aligned}&\mathcal{M}_j(\mathbf{k};n,l,m;\mathbf{v},D)\\&\quad=(2\pi)^{1/2}(K_j^{+}+a^{*}K_j^{-}+b^{*}K_j^{>})\ .\end{aligned} \tag{38}$$

The final step in the evaluation of $\mathcal{M}_j(\mathbf{k};n,l,m;\mathbf{v},D)$ now consists in the evaluation of the integrals $K_j^{\pm}$ and $K_j^{>}$. The factor $\exp(-iDq_z)$ entering the integrands $J_j^{\pm}(q_z)$ and $J_j^{>}(q_z)$ is, for $D>0$, an exponentially decreasing function in the *lower* half of the complex q_z plane. Complex contour integration may then be applied, provided the remainder of the integrand does not increase exponentially in the lower half-plane and has only a finite number of poles there.

In the integrands $J_j^{\pm}(q_z)$, the infinitesimal $i\eta$ shifts the pole of the factor $1/(q_z-p^{\pm}-i\eta)$ away from the real q_z axis into the upper half-plane, so that the analytic properties of $J_j^{\pm}(q_z)$ in the lower half-plane are solely decided by those of the function $F_j(q_z)$. The integrand $J_j^{>}(q_z)$ has in the lower half-plane a first-order pole at $q_z=p^{>}=-v_z-i\kappa_z$, apart from possible singularities of $F_j(q_z)$. We now turn to a detailed examination of the analytic structure of $F_j(q_z)$ for the specific forms (7) and (8) of the function $f_j(\mathbf{r}')$.

III. ANALYTIC STRUCTURE OF $F_j(q_z)$

The momentum-space representations $\tilde{f}_j(\mathbf{q})$ of the functions $f_j(\mathbf{r})$ corresponding to the overlap matrix elements ($j=1$) and the Coulomb matrix elements ($j=2$) are explicitly given in Appendix A. According to Eq. (26), the functions $F_j(q_z)$ are obtained by fixing in $\tilde{f}_j(\mathbf{q})$ the variables q_x and q_y to the values k_x' and k_y', respectively.

From Eq. (A3), it follows that $F_2(q_z)$ is related in a simple way to $F_1(q_z)$, viz.,

$$F_2(q_z)=-\tfrac{1}{2}(q_z^2+k_+'^2)F_1(q_z)\ , \tag{39}$$

where

$$k_+'=(k_\parallel'^2+\kappa_n^2)^{1/2}>0\ , \tag{40}$$

$$k_\parallel'=(k_x'^2+k_y'^2)^{1/2}\ , \tag{41}$$

and

$$\kappa_n=\frac{Z}{n}\equiv(-2\varepsilon_n)^{1/2} \tag{42}$$

is the parameter characterizing the decrease of the radial coordinate-space wave function $R_{nl}^{(Z)}(r)$ at large distances, i.e., $R_{nl}^{(Z)}(r)\propto\exp(-\kappa_n r)$ for $r\to\infty$. We can therefore confine ourselves to studying in detail the analytic structure of $F_1(q_z)$.

In view of Eq. (A5), we can write $F_1(q_z)$ in the factorized form

$$F_1(q_z)=(-i)^l U_{nl}^{(Z)}(q_z)W_{lm}(q_z)\ . \tag{43}$$

The functions $U_{nl}^{(Z)}(q_z)$ and $W_{lm}(q_z)$ are related to the radial momentum-space wave function $\tilde{R}_{nl}^{(Z)}(q)$ [cf. Eq. (A8)] and the momentum-space spherical harmonic $Y_{lm}(\theta_q,\phi_q)$ [cf. Eq. (A12)], respectively, by

$$U_{nl}^{(Z)}(q_z)\equiv\tilde{R}_{nl}^{(Z)}(q(q_z)) \tag{44}$$

and

$$W_{lm}(q_z)\equiv Y_{lm}(\theta_q(q_z),\phi_{k'})\ , \tag{45}$$

where

$$q(q_z)=(q_z^2+k_\parallel'^2)^{1/2}\ , \tag{46}$$

$$\cos\theta_q(q_z)=\frac{q_z}{q(q_z)}\ , \tag{47}$$

and

$$\tan\phi_{k'}=k_y'/k_x'\ . \tag{48}$$

More explicitly, we have from Eqs. (A8) and (A12)

$$U_{nl}^{(Z)}(q_z)=N_{nl}\frac{(q_z^2+k_\parallel'^2)^{l/2}}{(q_z^2+k_+'^2)^{l+2}}\,C_{n-l-1}^{l+1}\left[\frac{q_z^2+k_-'^2}{q_z^2+k_+'^2}\right]\ , \tag{49}$$

where

$$k_-'^2=k_\parallel'^2-\kappa_n^2 \tag{50}$$

and

$$W_{lm}(q_z)=\tilde{N}_{lm}\,P_l^m\left[\frac{q_z}{(q_z^2+k_\parallel'^2)^{1/2}}\right]\exp(im\phi_{k'})\ . \tag{51}$$

It is noted here that $k_-'^2$ can acquire both positive and negative values and accordingly k_-' itself can be purely real or purely imaginary. In the following derivation, however, only *even* powers of k_-' will be encountered.

Let us first consider the analytic structure of the functions $U_{nl}^{(Z)}(q_z)$ and $W_{lm}(q_z)$ separately.

Using the representation (49) of $U_{nl}^{(Z)}(q_z)$ and the explicit form (A10) of the Gegenbauer polynomial C_{n-l-1}^{l+1}, it is readily shown that $U_{nl}^{(Z)}(q_z)$ can be written as

$$U_{nl}^{(Z)}(q_z)=\frac{(q_z^2+k_\parallel'^2)^{l/2}}{(q_z^2+k_+'^2)^{n+1}}\mathcal{P}_{nl}(q_z)\ , \tag{52}$$

where the function $\mathcal{P}_{nl}(q_z)$ is a *polynomial* of degree $2(n-l-1)$ in q_z, whose explicit form is given in Appendix B. It is now immediately seen that in the lower half-plane $U_{nl}^{(Z)}(q_z)$ exhibits a pole of order $n+1$ at $q_z=-ik'_+$ [note that for bound ionic states, we have $\kappa_n>0$ and thus, according to Eq. (B1), $\mathcal{P}_{nl}(-ik'_+)\neq 0$]. Moreover, for *odd* values of the angular-momentum quantum number l, the factor $(q_z^2+k_\parallel'^2)^{l/2}$ gives rise, in the lower half-plane, to a branch point at $q_z=-ik'_\parallel\neq -ik'_+$.

Similarly, from the representation (51) of $W_{lm}(q_z)$ and the explicit form (A15) of the associated Legendre functions, it follows that $W_{lm}(q_z)$ can be written as

$$W_{lm}(q_z)=\frac{\mathcal{Q}_{lm}(q_z)}{(q_z^2+k_\parallel'^2)^{l/2}} , \tag{53}$$

where the function $\mathcal{Q}_{lm}(q_z)$ is a *polynomial* of degree $l-m$ in q_z, provided $k'_\parallel\neq 0$ or $k'_\parallel=0$ and $m=0$ [the explicit form of $\mathcal{Q}_{lm}(q_z)$ is given in Appendix B]. In this case, since $\mathcal{Q}_{lm}(-ik'_\parallel)\neq 0$ according to Eq. (B6), the function $W_{lm}(q_z)$ exhibits in the lower half-plane a pole of order $l/2$ at $q_z=-ik'_\parallel$ if l is *even*, and a branch point at $q_z=-ik'_\parallel$ if l is *odd*. If $k'_\parallel=0$ and $m\neq 0$, the overall factor $k_\parallel'^m$ in $\mathcal{Q}_{lm}(q_z)$ makes this function vanish identically. This feature reflects a selection rule for the matrix elements $\mathcal{M}_j$ following from the cylindrical symmetry of the functions $\phi_{\mathbf{k}}^{(V_0)}(\mathbf{r})\exp(-i\mathbf{v}\cdot\mathbf{r})$ for $k'_\parallel=0$. The analytic structure of $F_1(q_z)$ is now easily inferred from that of $U_{nl}(q_z)$ and $W_{lm}(q_z)$.

Inserting the expressions (52) and (53) into Eq. (43), one sees that the term $(q_z^2+k_\parallel'^2)^{l/2}$ in the denominator of $W_{lm}(q_z)$ cancels the identical term in the numerator of $U_{nl}(q_z)$, thereby removing the singularities associated with these terms. Hence we can write $F_1(q_z)$ as

$$F_1(q_z)=\frac{\mathcal{J}_1(q_z)}{(q_z^2+k_+'^2)^{n+1}} \equiv \frac{\mathcal{J}_1(q_z)}{(q_z-ik'_+)^{n+1}[q_z-(-ik'_+)]^{n+1}} , \tag{54}$$

where

$$\mathcal{J}_1(q_z)=(-i)^l\mathcal{P}_{nl}(q_z)\mathcal{Q}_{lm}(q_z) \tag{55}$$

is a polynomial of degree $2(n-1)-l-m$ in q_z. Using the condition $k'_+\geq\kappa_n$, it is easily shown from Eq. (B6) that $\mathcal{Q}_{lm}(-ik'_+)\neq 0$ and hence $\mathcal{J}_1(-ik'_+)\neq 0$. Therefore Eq. (54) reveals the key result of this section: in the lower half of the q_z plane, the function $F_1(q_z)$ exhibits a *single* pole, which is located at $q_z=-ik'_+$ and is of order $n+1$.

This simple result could not have been immediately anticipated. The appearance of a single pole characterized by the principal quantum number n only, and not of a manifold of distinct poles with order and position depending also on the angular-momentum quantum numbers l and m, apparently reflects the dynamical symmetry and the associated l degeneracy inherent in the hydrogen problem. The surprising feature is the prevalence of the dynamical symmetry even in a situation in which two of the coordinates of the momentum-space wave function are kept fixed. A more detailed investigation of the symmetry properties of the hydrogenic momentum-space wave functions will be necessary to understand this feature.

Turning now to the function $F_2(q_z)$, we can write, by using Eqs. (39) and (54),

$$F_2(q_z)=\frac{\mathcal{J}_2(q_z)}{(q_z-ik'_+)^n[q_z-(-ik'_+)]^n} , \tag{56}$$

where

$$\mathcal{J}_2(q_z)=-\tfrac{1}{2}\mathcal{J}_1(q_z) . \tag{57}$$

Hence, the only singularity of $F_2(q_z)$ in the lower half-plane is a pole at $q_z=-ik'_+$, i.e., at precisely the same position at which the pole of $F_1(q_z)$ shows up. The order of the pole of $F_2(q_z)$ is n, i.e., one unit less than that of the pole of $F_1(q_z)$.

In concluding this section, we write Eqs. (54) and (56) in the condensed form

$$F_j(q_z)=\frac{\mathcal{J}_j(q_z)}{(q_z-ik'_+)^{n-j+2}[q_z-(-ik'_+)]^{n-j+2}} , \quad j=1,2 , \tag{58}$$

which exhibits the property of $F_j(q_z)$ to have in the lower half-plane a single pole of order $n-j+2$ at $q_z=-ik'_+$. Equations (55) and (57) can be combined into

$$\mathcal{J}_j(q_z)=(-\tfrac{1}{2})^{j-1}(-i)^l\mathcal{P}_{nl}(q_z)\mathcal{Q}_{lm}(q_z) , \quad j=1,2 . \tag{59}$$

IV. EVALUATION OF MATRIX ELEMENTS

We are now prepared to evaluate the integrals $K_j^{\pm}$ and $K_j^{>}$ given by Eqs. (34) and (35) and finally the matrix elements (38).

A. The integrals $K_j^{\pm}$ and $K_j^{>}$

The position of the poles of the integrands $J_j^{\pm}(q_z)$ and $J_j^{>}(q_z)$ in the complex q_z plane is depicted schematically in Fig. 2. In the lower half-plane, the function $J_j^{\pm}(q_z)$ has a single pole of order $n-j+2$ at $q_z=-ik'_+$. The function $J_j^{>}(q_z)$ has two distinct poles, a first-order pole at $q_z=p^{>}$ and a pole of order $n-j+2$ at $q_z=-ik'_+$, provided $p^{>}\neq -ik'_+$. If the two poles coalesce at $q_z=-ik'_+$, a single pole of order $n-j+3$ emerges.

As the functions $F_j(q_z)$ and hence the functions $J_j^{\pm}(q_z)$ and $J_j^{>}(q_z)$ do not contain exponential parts, we can close the integration path in the integrals $K_j^{\pm}$ and $K_j^{>}$ in the lower half-plane. By applying the residue theorem (note that the integration contour $\mathcal{C}$ is defined in such a way that it encircles the poles in a *clockwise* sense), we obtain

$$K_j^{\pm}=\oint_{\mathcal{C}} dq_z J_j^{\pm}(q_z)=-2\pi i \operatorname{Res}_{q_z=-ik'_+}^{(n-j+2)} J_j^{\pm}(q_z) , \tag{60}$$

where the superscript $n-j+2$ indicates the order of the pole. Similarly, we have

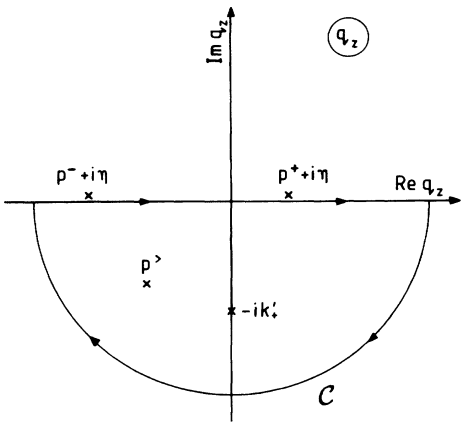

FIG. 2. Schematic diagram showing the distribution of poles of the functions $J_j^{\pm}(q_z)$ and $J_j^{>}(q_z)$ in the complex q_z plane and the integration contour $\mathcal{C}$ in the integrals $K_j^{\pm}$ and $K_j^{>}$.

$$K_j^{>}=\oint_{\mathcal{C}} dq_z J_j^{>}(q_z)$$
$$=-2\pi i[\mathrm{Res}^{(1)}_{q_z=p^{>}} J_j^{>}(q_z)+\mathrm{Res}^{(n-j+2)}_{q_z=-ik'_+} J_j^{>}(q_z)] \quad (61)$$

for $p^{>}\neq -ik'_+$, and

$$K_j^{>}=-2\pi i\,\mathrm{Res}^{(n-j+3)}_{q_z=-ik'_+} J_j^{>}(q_z) \quad (62)$$

for $p^{>}=-ik'_+$.

According to Eq. (31), the condition $p^{>}=-ik'_+$ can be fulfilled only if $v_z=0$. In this case, it acquires the form [cf. Eqs. (14) and (31)]

$$\kappa_z=k'_+ \quad (63)$$

and hence, according to Eqs. (9), (15), and (40),

$$\varepsilon_{k'}\equiv\varepsilon_{|\mathbf{k}-\mathbf{v}|}=\varepsilon_n \ . \quad (64)$$

The latter equation expresses, in the *rest frame* of the ion moving with velocity $\mathbf{v}=(v_x,v_y,0)$ parallel to the surface, the condition for *energy resonance* between metal electrons and ionic electrons. Note that energy resonance in the *laboratory system* cannot be achieved for $\mathbf{v}\neq 0$ (even if $v_z=0$) since in this case the ionic wave function with the translational factor included [cf. Eqs. (6) and (7)] is not an eigenfunction of the stationary ionic Hamiltonian. However, if $v_z=0$, the invariance of the metal Hamiltonian with respect to translations parallel to the surface allows the resonance condition to be established in the ion's rest frame.

B. Residues of $J_j^{\pm}(q_z)$ and $J_j^{>}(q_z)$

The evaluation of the residues in Eqs. (60), (61), and (62) is performed by applying the general formula [58]

$$\mathrm{Res}^{(\rho)}_{q_z=q_0} w(q_z)$$
$$=\frac{1}{(\rho-1)!}\frac{d^{\rho-1}}{dq_z^{\rho-1}}[w(q_z)(q_z-q_0)^{\rho}]\Big|_{q_z=q_0} \quad (65)$$

for a function $w(q_z)$ exhibiting a pole of order ρ at $q_z=q_0$.

The residue of $J_j^{>}(q_z)$ at the first-order pole at $q_z=p^{>}$, which appears in the *nonresonant* case $p^{>}\neq -ik'_+$, is accordingly given by

$$\mathrm{Res}^{(1)}_{q_z=p^{>}} J_j^{>}(q_z)$$
$$=i\exp(-iDp^{>})F_j(p^{>})$$
$$=i\frac{\exp(-iDp^{>})\mathcal{F}_j(p^{>})}{(k'_+ +ip^{>})^{n-j+2}(k'_+ -ip^{>})^{n-j+2}}$$
$$=i\frac{\exp[-D(\kappa_z-iv_z)]\mathcal{F}_j(-v_z-i\kappa_z)}{(k'_+ +\kappa_z-iv_z)^{n-j+2}(k'_+ -\kappa_z+iv_z)^{n-j+2}} \ , \quad (66)$$

i.e., it is expressed directly in terms of the ionic momentum-space wave function at *complex* values of the z component of the momentum.

In the *nonresonant* case $p^{>}\neq -ik'_+$, the evaluation of the residues of $J_j^{\pm}(q_z)$ and $J_j^{>}(q_z)$ at the pole of order $n-j+2$ at $q_z=-ik'_+$ is combined by writing

$$\mathrm{Res}^{(n-j+2)}_{q_z=-ik'_+} J_j(q_z)=\frac{i'}{(n-j+1)!}\frac{d^{n-j+1}}{dq_z^{n-j+1}}\left[\frac{\exp(-iDq_z)}{q_z-p}\frac{\mathcal{F}_j(q_z)}{(q_z-ik'_+)^{n-j+2}}\right]\Big|_{q_z=-ik'_+} \ , \quad (67)$$

where $J_j(q_z)$ stands for either $J_j^{\pm}(q_z)$ or $J_j^{>}(q_z)$, and correspondingly p for $p^{\pm}$ or $p^{>}$. The factor i' is equal to $-i$ in the "$\pm$" case, and equal to i in the "$>$" case. By successive differentiation, this expression is reduced to the form

$$\mathrm{Res}^{(n-j+2)}_{q_z=-ik'_+} J_j(q_z)=-i'\frac{\exp(-Dk'_+)}{(2k'_+)^{n-j+2}(k'_+ -ip)^{n-j+2}}$$
$$\times\mathcal{R}_j^{(n-j+2)}(k'_+,p;D) \ . \quad (68)$$

The "residue function" $\mathcal{R}_j^{(\rho)}(k'_+,p;D)$ corresponding to a pole of order ρ is defined as

$$\mathcal{R}_j^{(\rho)}(k'_+,p;D)=\sum_{\sigma=0}^{\rho-1}\left[1-i\frac{p}{k'_+}\right]^{\sigma}\mathcal{S}_j^{(\rho)}(\sigma;k'_+;D) \ , \quad (69)$$

where

$$\mathcal{S}_j^{(\rho)}(\sigma;k'_+;D)=\sum_{\tau=0}^{\sigma}\frac{(Dk'_+)^{\sigma-\tau}}{(\sigma-\tau)!}\mathcal{T}_j^{(\rho)}(\tau;k'_+) \ , \quad (70)$$

$$\mathcal{T}_j^{(\rho)}(\tau;k'_+)=\sum_{u=0}^{\tau}2^{-(\tau-u)}\begin{pmatrix}\rho-1+\tau-u\\ \rho-1\end{pmatrix}\mathcal{U}_j^{(u)}(k'_+) \ , \quad (71)$$

$$\mathcal{U}_j^{(u)}(k'_+)=\frac{(ik'_+)^u}{u!}\frac{d^u}{dq_z^u}\mathcal{F}_j(q_z)\bigg|_{q_z=-ik'_+} . \tag{72}$$

The specific arrangement of the various terms in Eq. (68) has been chosen in such a way that in the case $p=p^>$ the correspondence with similar terms in Eq. (66) is emphasized.

In the *strictly resonant* case $p^>=-ik'_+\equiv-i\kappa_z$, we obtain for the residue of $J_j^>(q_z)$ at the pole of order $n-j+3$ at $q_z=-ik'_+$

$$\begin{aligned}\mathrm{Res}_{q_z=-ik'_+}^{(n-j+3)} J_j^>(q_z)&=\frac{i}{(n-j+2)!}\frac{d^{n-j+2}}{dq_z^{n-j+2}}\left[\frac{\exp(-iDq_z)\mathcal{F}_j(q_z)}{(q_z-ik'_+)^{n-j+2}}\right]\bigg|_{q_z=-ik'_+}\\&=i\frac{\exp(-Dk'_+)}{(2k'^2_+)^{n-j+2}}\mathcal{S}_j^{(n-j+2)}(n-j+2;k'_+;D) .\end{aligned} \tag{73}$$

Looking at the dependence of the residues $\mathrm{Res}_{q_z=p^>}^{(1)}J_j^>(q_z)$ and $\mathrm{Res}_{q_z=-ik'_+}^{(n-j+2)}J_j^>(q_z)$, respectively, on the parameter $p^>$ (at fixed k'_+), we see from Eqs. (66) and (68) that in the vicinity of $p^>=-ik'_+$ the residues each vary as $[p^>-(-ik'_+)]^{-(n-j+2)}$. Therefore, if $p^>$ is arbitrarily close to $-ik'_+$, the integral $K_j^>$ [cf. Eq. (61)] cannot be accurately evaluated by summing the contributions calculated individually from the two residues. We can overcome this difficulty by showing that the *sum* of the residues is an analytic function of $p^>$ in the vicinity of $p^>=-ik'_+$, which can be expanded in a Taylor series about this point.

Writing

$$\begin{aligned}G_j^>(p^>)&=\mathrm{Res}_{q_z=p^>}^{(1)}J_j^>(q_z)+\mathrm{Res}_{q_z=-ik'_+}^{(n-j+2)}J_j^>(q_z)\\&\equiv\frac{H_j^>(p^>)}{[p^>-(-ik'_+)]^{n-j+2}} ,\end{aligned} \tag{74}$$

we have from Eqs. (66) and (68)

$$H_j^>(p^>)=i^{n-j+3}\left[\frac{\exp(-iDp^>)\mathcal{F}_j(p^>)}{(k'_++ip^>)^{n-j+2}}-\frac{\exp(-Dk'_+)\mathcal{R}_j^{(n-j+2)}(k'_+,p^>;D)}{(2k'_+)^{n-j+2}}\right] . \tag{75}$$

Using Eqs. (69) and (70), it is easily shown that the derivative of order α of the function $H_j^>(p^>)$ at $p^>=-ik'_+$ vanishes if $\alpha<n-j+2$, and is given by

$$\frac{d^\alpha}{dp^{>\alpha}}H_j^>(p^>)\bigg|_{p^>=-ik'_+}=i^{n-j+3}(-i)^\alpha\alpha!\frac{\exp(-Dk'_+)}{k'^\alpha_+(2k'_+)^{n-j+2}}\mathcal{S}_j^{(n-j+2)}(\alpha;k'_+;D) \tag{76}$$

if $\alpha\geq n-j+2$. Therefore, according to Eq. (74), the function $G_j^>(p^>)$ is analytic in the vicinity of $p^>=-ik'_+$, and its Taylor expansion in terms of the variable $p^>-(-ik'_+)\equiv-v_z+i(k'_+-\kappa_z)$ is obtained as

$$\begin{aligned}G_j^>(p^>)=&h_j^{(n-j+2)}+h_j^{(n-j+3)}[-v_z+i(k'_+-\kappa_z)]\\&+h_j^{(n-j+4)}[-v_z+i(k'_+-\kappa_z)]^2+\cdots ,\end{aligned} \tag{77}$$

where

$$h_j^{(\alpha)}=\frac{1}{\alpha!}\frac{d^\alpha}{dp^{>\alpha}}H_j^>(p^>)|_{p^>=-ik'_+} . \tag{78}$$

Note that the coefficient $h_j^{(n-j+2)}$ is identical (as it should be) to the expression (73) for the residue $\mathrm{Res}_{q_z=-ik'_+}^{(n-j+3)}J_j^>(q_z)$.

The evaluation of the residues of $J_j^\pm(q_z)$ and $J_j^>(q_z)$ can now be completed by evaluating the function $\mathcal{U}_j^{(u)}(k'_+)$ defined by Eq. (72). Using Eqs. (59), (B1), and (B6), the derivatives of the polynomial $\mathcal{F}_j(q_z)$ can be obtained by performing term-by-term differentiation of the polynomial resulting from multiplication of the polynomials $\mathcal{P}_{nl}(q_z)$ and $\mathcal{Q}_{lm}(q_z)$. Both from the point of view of a transparent formulation and of the numerical evaluation of the matrix elements, it is, however, advantageous to exploit the separable form (59) of the polynomial $\mathcal{F}_j(q_z)$ by writing

$$\begin{aligned}\frac{d^u}{dq_z^u}\mathcal{F}_j(q_z)=&(-\tfrac{1}{2})^{j-1}(-i)^l\sum_{v=0}^{u}\begin{bmatrix}u\\v\end{bmatrix}\frac{d^v}{dq_z^v}\mathcal{P}_{nl}(q_z)\\&\times\frac{d^{u-v}}{dq_z^{u-v}}\mathcal{Q}_{lm}(q_z)\end{aligned} \tag{79}$$

and performing term-by-term differentiation of the separate polynomials $\mathcal{P}_{nl}(q_z)$ and $\mathcal{Q}_{lm}(q_z)$. Introducing the functions

$$\mathcal{V}_{nl}^{(v)}(k'_+)=\frac{(ik'_+)^v}{v!}\frac{d^v}{dq_z^v}\mathcal{P}_{nl}(q_z)\bigg|_{q_z=-ik'_+} \tag{80}$$

$$\mathcal{W}_{lm}^{(w)}(k'_+)=\frac{(ik'_+)^w}{w!}\frac{d^w}{dq_z^w}\mathcal{Q}_{lm}(q_z)\bigg|_{q_z=-ik'_+}, \tag{81}$$

and we can write

$$\mathcal{U}_j^{(u)}(k'_+)=\begin{cases}(-\frac{1}{2})^{j-1}(-i)^l\sum_{v=0}^{u}\mathcal{V}_{nl}^{(v)}(k'_+)\mathcal{W}_{lm}^{(u-v)}(k'_+) & \text{if } u\le u_{\max}\\ 0 \text{ if } u>u_{\max}\ .\end{cases} \tag{82}$$

The explicit form of $\mathcal{V}_{nl}^{(v)}(k'_+)$ and $\mathcal{W}_{lm}^{(w)}(k'_+)$ is given in Appendix C. Since $\mathcal{F}_j(q_z)$ is a polynomial of degree $2(n-1)-l-m$, we have

$$u_{\max}=2(n-1)-l-m\ . \tag{83}$$

From Eq. (C11), it follows that $\mathcal{V}_{nl}^{(v)}(k'_+)$ is a *real* function. According to Eq. (C3), the function $\mathcal{W}_{lm}^{(w)}(k'_+)$ contains an overall phase factor $(-i)^{l+m}\exp(im\phi_{k'})$. Combining this factor with the factor $(-i)^l$ in the expression Eq. (82), it is seen that the function $\mathcal{U}_j^{(u)}(k'_+)$ contains an overall phase factor $(-)^{l+m}i^m\exp(im\phi_{k'})$. In the following, we assume that this factor is removed from $\mathcal{U}_j^{(u)}(k'_+)$ [and also from the function $\mathcal{F}_j(-v_z-i\kappa_z)$ appearing in Eq. (66)] and is incorporated into a prefactor of the matrix element $\mathcal{M}_j$. The functions $\mathcal{U}_j^{(u)}(k'_+)$ and $\mathcal{S}_j^{(\rho)}(\sigma;k'_+;D)$ are then purely real.

C. Complete expressions for the matrix elements

In this section we summarize the results of Secs. IV A and IV B to obtain final, closed-form expressions for the matrix elements (38), which exhibit the general structure of these quantities and their dependence on the relevant parameters. We assume at this point that the ion is located at an arbitrary position in the laboratory frame, specified by a position *vector* $\mathbf{D}$ (with z component $D_z\equiv D$). This introduces, in comparison with the form (38), an additional overall phase factor $\exp(-i\mathbf{D}_\parallel\cdot\mathbf{k}_\parallel)$ in the matrix elements, where $\mathbf{D}_\parallel$ and $\mathbf{k}_\parallel$ are the respective components of $\mathbf{D}$ and $\mathbf{k}$ parallel to the surface. Splitting the matrix elements into a contribution $\mathcal{M}_j^<$ from inside the metal (called henceforth the "metal contribution") and a contribution $\mathcal{M}_j^>$ from outside of the metal (the "vacuum contribution") and separating off the overall phase factor, we write for $m\ge 0$

$$\mathcal{M}_j(\mathbf{k};n,l,m;\mathbf{v},\mathbf{D})=(-1)^{l+m}\exp[i\phi_m(\mathbf{k},\mathbf{v};\mathbf{D})][\mathcal{M}_j^<(\mathbf{k};n,l,m;\mathbf{v},D)+\mathcal{M}_j^>(\mathbf{k};n,l,m;\mathbf{v},D)]\ , \tag{84}$$

where

$$\mathcal{M}_j^<(\mathbf{k};n,l,m;\mathbf{v},D)=(2\pi)^{1/2}(K_j^+ + a^* K_j^-)\ , \tag{85}$$

$$\mathcal{M}_j^>(\mathbf{k};n,l,m;\mathbf{v},D)=(2\pi)^{1/2}b^* K_j^>\ , \tag{86}$$

and

$$\phi_m(\mathbf{k},\mathbf{v};\mathbf{D})=m\left[\phi_{k'}+\frac{\pi}{2}\right]-\mathbf{D}_\parallel\cdot\mathbf{k}_\parallel\ . \tag{87}$$

For the *metal* contribution at arbitrary parameter values, we obtain from Eqs. (60) and (68)

$$\mathcal{M}_j^<(\mathbf{k};n,l,m;\mathbf{v},D)=(2\pi)^{3/2}\frac{\exp(-Dk'_+)}{(2k'_+)^{n-j+2}}\left[\frac{\mathcal{R}_j^{(n-j+2)}(k'_+,k_z-v_z;D)}{[k'_+-i(k_z-v_z)]^{n-j+2}}+a^*\frac{\mathcal{R}_j^{(n-j+2)}(k'_+,-k_z-v_z;D)}{[k'_++i(k_z+v_z)]^{n-j+2}}\right]. \tag{88}$$

The *vacuum* contribution in the nonresonant case $p^>\equiv -v_z-i\kappa_z\neq -ik'_+$ follows from Eqs. (61), (66), and (68) as

$$\mathcal{M}_j^>(\mathbf{k};n,l,m;\mathbf{v},D)=(2\pi)^{3/2}\frac{b^*}{(k'_+-\kappa_z+iv_z)^{n-j+2}}\times\left[\frac{\exp[-D(\kappa_z-iv_z)]\mathcal{F}_j(-v_z-i\kappa_z)}{(k'_++\kappa_z-iv_z)^{n-j+2}}-\frac{\exp(-Dk'_+)\mathcal{R}_j^{(n-j+2)}(k'_+,-v_z-i\kappa_z;D)}{(2k'_+)^{n-j+2}}\right]. \tag{89}$$

To deal with the vacuum contribution in the near-resonant case (including the strictly resonant case $p^>=-ik'_+$), we can combine Eqs. (61), (74), and (77) to obtain an expansion of $\mathcal{M}_j^>$ in terms of the dimensionless variable $(k'_+-\kappa_z+iv_z)/k'_+$:

$$\mathcal{M}_j^{>}(\mathbf{k};n,l,m;\mathbf{v},D)=(2\pi)^{3/2}b^*\frac{\exp(-Dk'_+)}{(2k'^2_+)^{n-j+2}}\left[\mathcal{S}_j^{(n-j+2)}(n-j+2;k'_+;D)+\mathcal{S}_j^{(n-j+2)}(n-j+3;k'_+;D)\frac{k'_+-\kappa_z+iv_z}{k'_+}\right.$$
$$\left.+\mathcal{S}_j^{(n-j+2)}(n-j+4;k'_+;D)\left[\frac{k'_+-\kappa_z+iv_z}{k'_+}\right]^2+\cdots\right]. \quad (90)$$

In the strictly resonant case, we recover from Eq. (90) that expression for the matrix element $\mathcal{M}_j^{>}$ which follows directly from Eqs. (62), (73), and (86). If $v_z=0$, we can introduce, in generalization of Eq. (64), the "energy defect"

$$\Delta=\varepsilon_{k'}-\varepsilon_n\equiv\tfrac{1}{2}(k'^2_+-\kappa_z^2) \quad (91)$$

to rewrite the expansion variable in Eq. (90) as

$$\frac{k'_+-\kappa_z}{k'_+}=1-\left[1-\frac{2\Delta}{k'^2_+}\right]^{1/2}$$
$$=\frac{\Delta}{k'^2_+}\left[1+\frac{\Delta}{2k'^2_+}+\cdots\right]. \quad (92)$$

The matrix element $\mathcal{M}_j^{>}$ thus varies, for fixed k'_+ and small Δ, linearly with Δ.

We do not enter here a discussion of the convergence properties of the expansion (90). From a practical point of view, the expansion is needed to evaluate the matrix element $\mathcal{M}_j^{>}$ in the immediate vicinity of the energy resonance, where the numerical evaluation of the exact expression (89) is bound to fail. It can be assumed that an evaluation of the first-order term of the expansion is sufficient for an accurate interpolation of $\mathcal{M}_j^{>}$ in that range where the numerical results obtained from the exact expression look irregular.

From the expressions (88), (89), and (90), some qualitative insight into the structure of $\mathcal{M}_j^{<}$ and $\mathcal{M}_j^{>}$ can be gained. The metal contribution $\mathcal{M}_j^{<}$ given by Eq. (88) exhibits a particularly simple dependence on the ion-surface distance D, viz., a dependence solely via the dimensionless parameter Dk'_+, with a polynomial in this parameter arising from the function $\mathcal{S}_j^{(\rho)}(\sigma;k'_+;D)$, and a common factor $\exp(-Dk'_+)$ governing the behavior of $\mathcal{M}_j^{<}$ at large distances D. At fixed (large) D, the presence of the factor k'_+ in the exponential entails a falloff of $|\mathcal{M}_j^{<}|$ both as a function of the binding energy $|\varepsilon_n|$ of the ionic state and as a function of the parallel momentum $k'_\parallel$ of the conduction-band electron relative to the moving ion. The binding-energy dependence reflects the decreasing spatial overlap of the ionic wave function with the conduction-band wave function inside the metal. Similarly, the momentum dependence reflects the increasing mismatch between conduction-band momentum and the momentum distribution in the ionic state.

The dependence of $\mathcal{M}_j^{<}$ on the momentum component k_z (at fixed k'_+) is, according to Eqs. (69) and (88), a polynomial dependence in the variables $1/(k_z-v_z+ik'_+)$ and $1/(k_z+v_z-ik'_+)$, respectively, for the "incoming" and the "reflected" part in Eq. (88). The nonappearance of an exponential dependence on k_z is plausible since the incoming and reflected plane-wave parts of the jellium wave function are "cut off" at the surface. Accordingly they are not eigenfunctions of the momentum operator with respect to the interval $-\infty<z<+\infty$, but correspond to the broad momentum distribution given by Eq. (32), whose overlap with the ionic momentum distribution is expected to vary slowly with the parameters.

The ion velocity in the laboratory frame, $\mathbf{v}$, enters the matrix element $\mathcal{M}_j^{<}$ in an obvious way by shifting the momentum components of the conduction-band electron from their values in the laboratory frame (with the z component taken as $\pm k_z$, corresponding to the incoming and reflected part of the jellium wave functions; the reflection coefficient a is *not* affected by the ion velocity) to values referred to the ion-centered frame. In the specific case $v_z=0$, it is easily shown from Eq. (69) that

$$\mathcal{R}_j^{(n-j+2)}(k'_+,-k_z;D)=\mathcal{R}_j^{(n-j+2)*}(k'_+,k_z;D), \quad (93)$$

and hence $K_j^-=K_j^{+*}$, so that $\mathcal{M}_j^{<}$ acquires the simplified form

$$\mathcal{M}_j^{<}(\mathbf{k};n,l,m;\mathbf{v},D)=(2\pi)^{1/2}(K_j^+ + a^*K_j^{+*}). \quad (94)$$

Using Eq. (19), this can be rewritten as

$$\mathcal{M}_j^{<}(\mathbf{k};n,l,m;\mathbf{v},D)$$
$$=2(2\pi)^{1/2}\exp(-i\chi_a)\mathrm{Re}[K_j^+\exp(i\chi_a)]. \quad (95)$$

The phase of $\mathcal{M}_j^{<}$ at $v_z=0$ is thus given by $-\chi_a$ or $-\chi_a\pm\pi$, depending on whether $\mathrm{Re}[K_j^+\exp(i\chi_a)]$ is positive or negative.

The vacuum contribution $\mathcal{M}_j^{>}$ exhibits a more complicated D dependence than does the metal contribution $\mathcal{M}_j^{<}$. At large distances, the behavior of $\mathcal{M}_j^{>}$ is dominated by the first or second term in the large parentheses of Eq. (89), depending on whether $\kappa_z<k'_+$ or $\kappa_z>k'_+$. The dependence on κ_z (at fixed k'_+), i.e., the dependence on k_z, is particularly involved in the near-resonant case, in which the singular behavior of the negative power of $k'_+-\kappa_z+iv_z$ in Eq. (89) is compensated by the vanishing of the large parentheses.

The ion velocity $\mathbf{v}$ affects $\mathcal{M}_j^{>}$ by shifting the momentum components in the laboratory frame, where $i\kappa_z$ is now to be considered as the z component, to their values in the ion-centered frame (the penetration coefficient b is not affected by the ion velocity). In the case $v_z=0$ (which includes the strictly resonant case), it follows from Eq. (89) that $\mathcal{M}_j^{>}$ is given as a product of a real function and the penetration factor b^*. Now, by using Eqs. (22) and (95) we can infer that the *relative* phase between $\mathcal{M}_j^{<}$ and $\mathcal{M}_j^{>}$ at $v_z=0$ is either 0 or $\pm\pi$. This result has the important consequence that the metal contribution and the vacuum contribution interfere either *completely constructive* or *completely destructive* when the total matrix element is

formed.

In the strictly resonant case, the *total* matrix element $\mathcal{M}_j$ involves an overall factor $\exp(-Dk'_+)\equiv\exp(-D\kappa_z)$. This implies that the falloff of the matrix element at large D is solely determined by that parameter which characterizes the exponential falloff of the jellium wave function in the vacuum region (or, equivalently, by the momentum component k_z).

The matrix elements corresponding to $m<0$ can be readily expressed in terms of those for $m>0$. Using Eqs. (5)–(8), (23), and (A13), we obtain

$$\mathcal{M}_j(\mathbf{k};n,l,-m;\mathbf{v},\mathbf{D})=(-1)^m\mathcal{M}_j^*(-\mathbf{k};n,l,m;-\mathbf{v},\mathbf{D}) . \tag{96}$$

Further, from inspecting Eqs. (87)–(89), we have

$$\mathcal{M}_j^<(-\mathbf{k};n,l,m;-\mathbf{v},D)=\mathcal{M}_j^{<\,*}(\mathbf{k};n,l,m;\mathbf{v},D) , \tag{97}$$

$$\mathcal{M}_j^>(-\mathbf{k};n,l,m;-\mathbf{v},D)=\mathcal{M}_j^{>\,*}(\mathbf{k};n,l,m;\mathbf{v},D) , \tag{98}$$

and

$$\phi_m(-\mathbf{k},-\mathbf{v};\mathbf{D})=-\phi_{-m}(\mathbf{k},\mathbf{v};\mathbf{D}) . \tag{99}$$

Hence, using Eq. (84),

$$\mathcal{M}_j(\mathbf{k};n,l,-m;\mathbf{v},\mathbf{D}) =(-1)^m\exp\{i[\phi_{-m}(\mathbf{k},\mathbf{v};\mathbf{D})-\phi_m(\mathbf{k},\mathbf{v};\mathbf{D})]\} \times\mathcal{M}_j(\mathbf{k};n,l,m;\mathbf{v},\mathbf{D}) , \tag{100}$$

i.e., the matrix elements for $m=-|m|<0$ differ from those for $m=|m|$ merely by a phase factor.

Except for the overall phase factor $\exp(im\phi_{k'})$, the matrix elements $\mathcal{M}_j$ depend on the momentum components k'_x and k'_y only via $k'_\parallel$. Accordingly, $|\mathcal{M}_j|$ is invariant under rotations about the z axis in $\mathbf{k}'$ space and depends on $k'_\parallel$ and $k'_z=\pm k_z-v_z$ only.

The only *selection rule* for the matrix elements $\mathcal{M}_j$ appears to be

$$\mathcal{M}_j=0 \quad \text{if } k'_\parallel=0 \text{ and } m\neq 0 , \tag{101}$$

which originates from the factor $k'^m_\parallel$ in Eq. (B7) and which expresses the cylindrical symmetry of the functions $\phi_{\mathbf{k}}^{(V_0)}(\mathbf{r})\exp(-i\mathbf{v}\cdot\mathbf{r})$ for $k'_\parallel=0$. We are not aware of any general *scaling law* connecting the values of the matrix elements at different parameter values.

We note here again that the matrix elements corre-

This relation can be exploited to crosscheck the numerical results.

While the condition $D>0$ had to be imposed in order to allow the q_z integration in the integrals $K_j^{\pm}$ and $K_j^>$ to be performed by contour integration in the lower half-plane, the resulting expressions for the matrix elements $\mathcal{M}_j$ are readily seen to be well defined at $D=0$ and equal to $\lim_{D\to 0}\mathcal{M}_j$.

D. Numerical evaluation

While the expressions (88) and (89) constitute truly closed-form expressions for the matrix elements $\mathcal{M}_j^<$ and $\mathcal{M}_j^>$, some care is required in their actual evaluation (which, except for very simple limiting cases, must be performed by numerical computation). For large values of the ionic principal quantum number n, the summation of the residue function $\mathcal{R}_j^{(n-j+2)}(k'_+,p;D)$ may involve an enormously large number of terms. Precautions must then be taken to avoid unacceptably large round-off errors and computing time.

From Eqs. (69)–(71) and (82), it follows that the evaluation of the function $\mathcal{R}_j^{(n-j+2)}(k'_+,p;D)$ involves, for given product $\mathcal{V}_{nl}^{(v)}(k'_+)\mathcal{W}_{lm}^{(u-v)}(k'_+)$, a fourfold "outer" summation (over indices σ,τ,u,v). The number of terms in this sum is estimated to be of order $n^4/8$. The number of terms in the threefold sum occurring in the function $\mathcal{V}_{nl}^{(v)}(k'_+)$ of Eq. (C1) depends, at given n, strongly on the value of l. It is found by explicit calculation that the maximum number of terms is roughly given by $f(n)n^2$, where $f(n)$ is a monotonic function that increases slowly with n and attains a value of about 8 at $n=100$. The number of terms in the twofold sum in $\mathcal{W}_{lm}^{(w)}(k'_+)$ is very small in comparison with the maximum number of terms in $\mathcal{V}_{nl}^{(v)}(k'_+)$. It is noted here that an evaluation of the function $\mathcal{U}_j^{(u)}(k'_+)$ not from Eq. (82), but from the "multiplied" form of the polynomial $\mathcal{F}_j(q_z)$ [cf. the discussion preceding Eq. (80)] would result in a fivefold sum and accordingly entail a larger total computing time for the matrix element.

To evaluate $\mathcal{R}_j^{(n-j+2)}(k'_+,p;D)$ for a given set of parameter values, it is advisable to compute and store $\mathcal{V}_{nl}^{(v)}(k'_+)$ and $\mathcal{W}_{lm}^{(w)}(k'_+)$ for the required range of indices v and w and subsequently perform the sums over v, u, τ, and σ. For specific parameter values, it may of course be advantageous to rearrange the expression for $\mathcal{R}_j^{(n-j+2)}(k'_+,p;D)$ and perform the sums in a different

and to avoid overflows in the numerical summation of $\mathcal{R}_j^{(n-j+2)}(k'_+,p;D)$ by avoiding the appearance of excessively large numbers in the computer. One source of large numbers could be the factorials which are present in the normalization factors (A9) and (A14) as well as in the Gegenbauer polynomials (A10), and also those which arise from the successive differentiations encountered in the evaluation of the residues of the functions $J_j(q_z)$. Therefore, the coefficients in the functions (70), (71), (82), (C1), and (C3) defining the final expression for $\mathcal{R}_j^{(n-j+2)}(k'_+,p;D)$ have been written in a way in which factorials have been absorbed, whenever possible, into binomial coefficients. It is seen that the only remaining factorial shows up in the function $\mathcal{S}_j^{(\rho)}(\sigma;k'_+;D)$ of Eq. (70). The binomial coefficients are of reasonable magnitude even for very large quantum numbers n.

Another possible source of large numbers are the powers of Dk'_+ occurring in the function $\mathcal{S}_j^{(\rho)}(\sigma;k'_+;D)$, which can be exceedingly large if both D and n are large. This problem can be conveniently dealt with by combining the powers $(Dk'_+)^\mu$ with the function $\exp(-Dk'_+)$ of Eq. (68) and the factorial of Eq. (70) into a single function $(Dk'_+)^\mu\exp(-Dk'_+)/\mu!$. This function can be shown to be always smaller than unity and can be accurately evaluated by applying a recurrence relation for its logarithm.

Finally, by expressing the components of $\mathbf{k}$ and $\mathbf{v}$ as well as κ_z and κ_n in terms of multiples of k'_+, we can avoid the appearance of large values of powers involving these quantities. When scaled with k'_+, the quantities k'_-, $k'_\parallel$, and κ_n are smaller than unity. Expressed in terms of the scaled quantities, the matrix elements appear as a dimensionless part multiplied by a factor $k'^{2j-7/2}_+$.

V. EXAMPLES AND DISCUSSION

The large number of parameters in the matrix elements renders difficult a systematic survey of their properties. When considering here explicit examples, we have to confine ourselves to a few typical cases which are selected partly according to their value for demonstrating the potentialities of our method and partly according to their relevance for applications.

Throughout this section we will consider the case $\mathbf{v}=0$ only. While a nonzero velocity component of the ion *parallel* to the surface results in a trivial kinematic transformation in the matrix elements, the conditions of present-day experiments are indeed in most cases near-adiabatic with respect to the motion of the ion *normal* to the surface. The case $v_z=0$ is thus an important limiting case. In the adiabatic limit $\mathbf{v}=0$, the total electronic energy is conserved in transitions between conduction-band states and ionic states. Then only matrix elements corresponding to the strictly resonant case are of physical importance, and we restrict our examples essentially to this case. In order to illustrate the behavior of the matrix elements in the nonresonant case, we consider in a few examples their dependence on the energy defect Δ introduced in Eq. (91).

In the graphical representations of the matrix elements as a function of the ion-surface distance D, we will indicate the value D_0 at which the top of the potential barrier between metal and ion coincides with ionic level under consideration. From Eqs. (3), (4), and (9), it follows that

$$D_0=\frac{Z}{|\varepsilon_n|}=\frac{2n^2}{Z}\ . \tag{103}$$

The distance D_0 (the "classical threshold") separates the "classically allowed" range in which resonant electron transfer is classically possible, from the "classically forbidden" range where this transfer can be effected by quantal tunneling only. In the classically forbidden range, a rapid (exponential) decrease of overlap and Coulomb matrix elements can be anticipated.

For the sake of simplicity, the depth of the conduction-band potential is taken in the following examples (except for one case) as $V_0=0.5$ a.u. $\hat{=}$ 13.605 eV. This value is slightly larger than the average of the experimental values for the metals usually used in studies of ion–metal-surface scattering. We consider two choices for the ionic states, viz., the $n=8$ manifold at $Z=5$ and the $n=14$ manifold at $Z=9$. The binding energies of the corresponding ionic levels are 5.31 and 5.62 eV, respectively, which is roughly equal to the electronic binding energy at the Fermi level of the conduction band.

A. The case $\Delta=0$, $k_\parallel=0$

We begin our discussion of the properties of the matrix elements $\mathcal{M}_j$ by considering the resonant case ($\Delta=0$) at $k_\parallel=0$. The selection rule (101) restricts the nonzero matrix elements in this case to those with $m=0$. Then, according to Eq. (84), the overall phase factor in $\mathcal{M}_j$ is equal to $(-1)^l$.

In Figs. 3–7 results are displayed for $Z=5$, $n=8$, $l=0$, and $V_0=0.5$ a.u. The momentum component k_z is fixed, by energy conservation, to the value 0.781 a.u.

In Fig. 3 the real and imaginary parts of the metal contribution $\mathcal{M}_1^<$ and of the vacuum contribution $\mathcal{M}_1^>$ to the overlap matrix element $\mathcal{M}_1$ are shown as a function of the ion-surface distance D. The common features of the curves are oscillatory behavior in the classically allowed range $D<D_0$ and exponential falloff in the classically for-

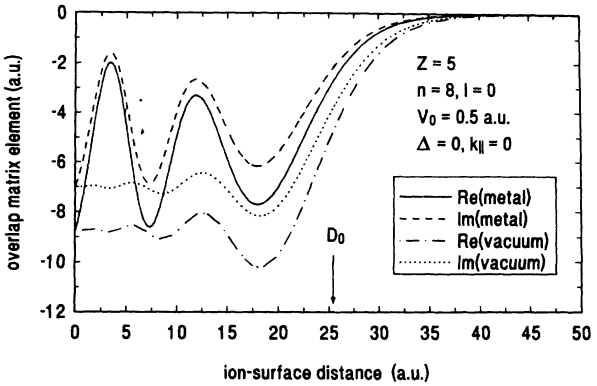

FIG. 3. Real and imaginary parts of the metal and vacuum contributions to the overlap matrix element for $Z=5$, $n=8$, $l=0$, $V_0=0.5$ a.u., $\Delta=0$, $k_\parallel=0$, plotted as a function of the ion-surface distance D.

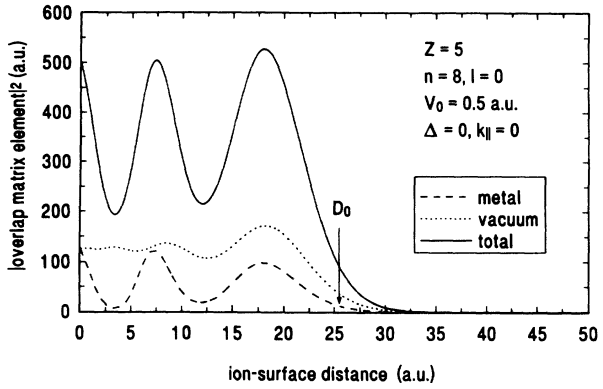

FIG. 4. Square modulus of the overlap matrix elements shown in Fig. 3.

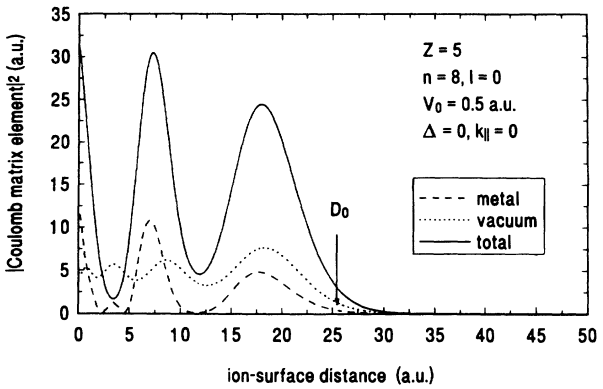

FIG. 6. Square modulus of the Coulomb matrix elements shown in Fig. 5.

bidden range $D > D_0$. This behavior is representative for all our results. The oscillations in the metal and vacuum contribution bear certain similarities to each other, with a tendency of the metal contribution to show more pronounced oscillations. The frequency of the oscillations appears to be somewhat larger in the vacuum contribution. While the occurrence of the oscillations is clearly related to the nodal structure of the ionic wave functions and, in the case of the metal contribution, also to the oscillatory behavior of the z-dependent part of the jellium wave function, it appears that no simple rule for the number of maxima and minima can be given. In general, this number turns out to be considerably smaller than what would be anticipated from the number of radial nodes of the ionic wave function, and/or from the wavelengths of the jellium wave functions. Further analysis will be necessary to clarify this situation. It is noted that the confluence at $D=0$ of the curves pertaining to the real parts of metal and vacuum contribution and those pertaining to the imaginary parts is purely accidental.

Closer inspection of the results shown in Fig. 3 reveals that the complex phase of the metal contribution is independent of D and equal to $-\chi_a+\pi$, in conformity with Eq. (95). The phase of the vacuum contribution is identical to that of the metal contribution for all D values, so that the condition imposed on the relative phase between vacuum and metal contribution (cf. the discussion in Sec. IV C) is fulfilled. In Fig. 4 the square moduli of metal and vacuum contribution and of the total overlap matrix element are displayed, exhibiting indeed constructive interference between metal and vacuum contribution throughout. The absolute magnitudes of metal and vacuum contribution are seen to be of the same order in the classically allowed range, whereas the metal contribution decreases much faster than the vacuum contribution in the range close to and beyond the classical threshold. This tendency has been observed throughout our calculations.

The Coulomb matrix elements displayed in Figs. 5 and 6 bear a close resemblance to the overlap matrix elements of Figs. 3 and 4 with regard to their qualitative features. A noteworthy discrepancy occurs in the range $2.4 < D < 4.5$ a.u., in which the relative phase between vacuum and metal contribution is equal to π, thereby giving rise to destructive interference between these contributions.

The similarities and differences between Coulomb and overlap matrix elements become more apparent from Fig. 7, in which ratios of various combinations of the contri-

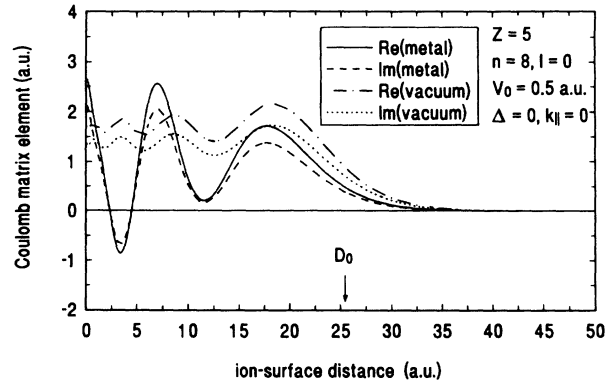

FIG. 5. Real and imaginary parts of the metal and vacuum contributions to the Coulomb matrix element for $Z=5$, $n=8$, $l=0$, $V_0=0.5$ a.u., $\Delta=0$, $k_{\parallel}=0$, plotted as a function of the ion-surface distance D.

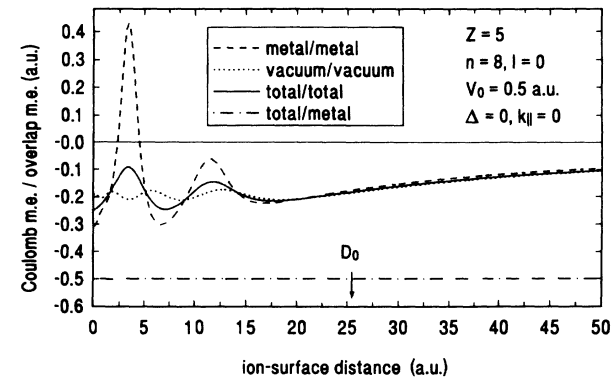

FIG. 7. Ratios of various contributions to the Coulomb and overlap matrix elements shown in Figs. 5 and 3, respectively.

butions to these matrix elements are shown as a function of ion-surface distance. The ratio of the metal contributions reflects the rapid fluctuations of the individual contributions in the classically allowed region. The ratio of the vacuum contributions displays a weak dependence on D over the full D range, with modulations in the classically allowed range which are apparently smaller than in the individual contributions. The average value of the ratios of the vacuum contributions as well as that of the ratios of the total matrix elements is about -0.2 a.u., which is close to the energy $\varepsilon_n = -0.195$ a.u. of the ionic state with $Z=5$, $n=8$. This near-quality is plausible in view of Eq. (A3), from which the average ratio of the momentum-space functions $\tilde{f}_2(\mathbf{q})$ and $\tilde{f}_1(\mathbf{q})$ and consequently that of the matrix elements $\mathcal{M}_2$ and $\mathcal{M}_1$ is estimated to be of order ε_n. The near-equality of the ratio of the metal contributions and the ratio of the vacuum contributions in the classically forbidden range appears to be an accidental feature. The ratio of the total Coulomb matrix element to the metal contribution to the overlap matrix element is seen to have the constant value -0.5 a.u., in conformity with Eq. (102).

We now turn to the dependence of the matrix elements on the ionic orbital angular-momentum quantum number l. Because of the similarities between overlap and Coulomb matrix elements and their simple phase properties, we confine ourselves in the following to the discussion of the square moduli of Coulomb matrix elements.

In Fig. 8 the square modulus of the Coulomb matrix element for $Z=5$, $n=8$, $m=0$, $V_0=0.5$ a.u. is shown as a function of D for $l=0,2,5,7$. The results exhibit an increasingly stronger localization of the matrix elements in the range of small distances when the l value increases. In a classical picture, this feature can be understood in terms of the eccentricity of the ionic Kepler orbits. Low l values imply large eccentricity and hence large penetration of the orbit into the metal even at large distances. The eccentricity of high-l orbits is small, so that substantial penetration into the metal occurs in this case at small D values only. From a quantal point of view, the trend observed in Fig. 8 is understood in terms of the root-mean-square radius of the ionic wave function, which decreases with increasing l, thus giving rise to a progressively smaller overlap of the wave function with the metal.

For very large principal quantum numbers n, the localization of the matrix elements at small ion-surface distances does not become monotonically stronger with increasing l. In Fig. 9 we show the D dependence of the square modulus of the Coulomb matrix element for $Z=9$, $n=14$, $m=0$, $V_0=0.5$ a.u. ($k_z=0.766$ a.u.), and $l=0,1,2,3$. The $l=1$ and 2 matrix elements are seen to be stronger localized in the range close to the classical threshold D_0 than is the $l=0$ matrix element. Only for $l>2$, a tendency towards a monotonic shift of the localization to smaller distances develops. Such a behavior of the matrix elements apparently reflects subtle structural properties of the ionic wave function. To achieve a better understanding of this situation, a more detailed analysis will be necessary.

The influence of the depth V_0 of the jellium potential is illustrated by Fig. 10, where results are shown for $Z=9$, $n=14$, $l=0$, and different V_0 values. When V_0 varies between 0.3 and 0.6 a.u., the momentum component k_z varies between 0.432 and 0.887 a.u. With increasing V_0, an overall reduction of the magnitude of the matrix elements is observed. Further, the wavelength of the oscillations becomes progressively smaller, particularly at small distances, where a reduction by roughly a factor of 2 is observed when V_0 changes from its smallest to its largest value. This factor is close to the relative change of $1/k_z$, i.e., of the wavelength of the z-dependent part of the jellium wave function inside the metal. This suggests a correlation between the oscillations in the jellium wave function and those in the matrix elements at small ion-surface distances. In a complete analysis of this point, the metal and vacuum contributions to the matrix elements will have to be considered separately.

B. The case $\Delta=0$, $k_\parallel \neq 0$

In this section we study the dependence of the matrix elements on the conduction-band momentum for the res-

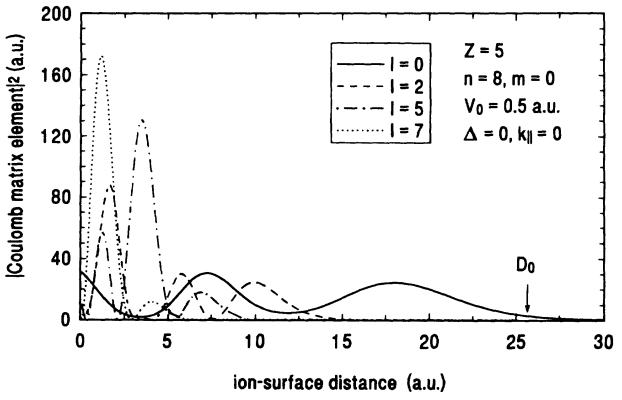

FIG. 8. Square modulus of the Coulomb matrix element for $Z=5$, $n=8$, $m=0$, $V_0=0.5$ a.u., $\Delta=0$, $k_\parallel=0$, plotted as a function of the ion–square-distance D for various values of the orbital angular-momentum quantum number l.

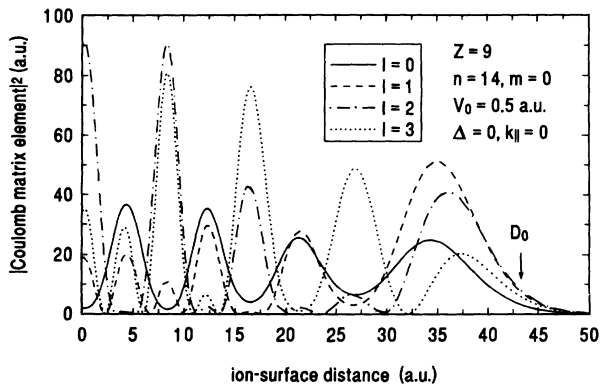

FIG. 9. Square modulus of the Coulomb matrix element for $Z=9$, $n=14$, $m=0$, $V_0=0.5$ a.u., $\Delta=0$, $k_\parallel=0$, plotted as a function of the ion–surface-distance D for various values of the orbital angular-momentum quantum number l.

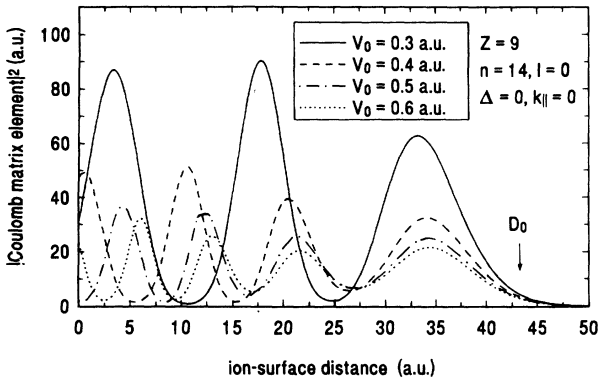

FIG. 10. Square modulus of the Coulomb matrix element for $Z=9$, $n=14$, $l=0$, $\Delta=0$, $k_{\parallel}=0$, plotted as a function of the ion–surface-distance D for various values of the depth V_0 of the conduction-band potential.

onant case $\Delta=0$. As the magnitude of the momentum vector $\mathbf{k}$ is fixed by energy conservation and $|\mathcal{M}_j|$ is invariant under rotations about the z axis in $\mathbf{k}$ space, we can choose to discuss the matrix elements as a function of $k_{\parallel}$, the component k_z being related to $k_{\parallel}$ via

$$k_z=[2(V_0+\varepsilon_n)-k_{\parallel}^2]^{1/2}\ . \tag{104}$$

For $k_{\parallel}\neq 0$, the magnetic quantum number m is an additional parameter whose influence on the matrix elements can be investigated. Since, according to Eq. (100), $|\mathcal{M}_j|$ is independent of the sign of m, we can confine ourselves to the case $m\geq 0$.

In Fig. 11 the D and $k_{\parallel}$ dependence of the square modulus of the Coulomb matrix element for $Z=5$, $n=8$, $l=0$, $V_0=0.5$ a.u. is shown in a three-dimensional plot covering the full range of allowed $k_{\parallel}$ values. Oscillatory behavior is observed in both coordinate directions. The onset of the exponential falloff as a function of D, which is located roughly at the classical threshold D_0 when $k_{\parallel}=0$, is seen to shift to progressively smaller distances when $k_{\parallel}$ increases. This feature reflects the overall factor $\exp[-2D(k_{\parallel}^2+\kappa_n^2)^{1/2}]$ in $|\mathcal{M}_j|^2$ (cf. the discussion in Sec. IV C).

The D and $k_{\parallel}$ dependence for the parameters of Fig. 11, but $l=7$, $m=0$ is displayed in Fig. 12. The matrix element is now strongly localized in the vicinity of $D=0$, $k_{\parallel}=0$. While the compression towards small D is plausible in view of the arguments given in the discussion of Fig. 8, the localization in the vicinity of $k_{\parallel}=0$ is not obvious. The spatial distribution of the ionic wave functions at large l values is characterized by a strong elongation along the z axis (i.e., along the surface normal) for small values of $|m|$ ("cigarlike" shape), and a compression along this axis for large values of $|m|$ ("pancakelike shape"). For sufficiently large distances D, these features imply a decreasing penetration of the ionic wave function into the metal when $|m|$ increases. The corresponding momentum-space wave functions are expected to be fairly delocalized parallel to the surface when $|m|$ is small, and localized in the range of small $k_{\parallel}$ when $|m|$ is large. The fact that the matrix elements of Fig. 12 oscillate, in the range beyond $D\simeq 5$ a.u., about a roughly *constant* mean value when considered as a function of $k_{\parallel}$ can now be understood as resulting from the properties of the $m=0$ momentum-space wave function. The situation in the small-D range appears to be more intricate.

The matrix elements for the case of Fig. 12, but $m=7$, are shown in Fig. 13. Now a single broad maximum in the small-D range appears, which is centered about $k_{\parallel}\simeq 0.5$ a.u. and whose peak value is much smaller than that of the main peak in Fig. 12 (note the difference in scale for the matrix elements in Figs. 12 and 13). The simple geometrical structure of the landscape shown in Fig. 13 apparently reflects the absence of (radial and polar) nodes in the ionic wave function. The maximum shows up at larger $k_{\parallel}$ values than would be expected from the momentum-space arguments given above (which, however, are barely applicable at such small distances).

In Figs. 14 and 15 we show the square modulus of the Coulomb matrix elements for the case $Z=9$, $n=14$, $V_0=0.5$ a.u. The purpose of studying this case is not

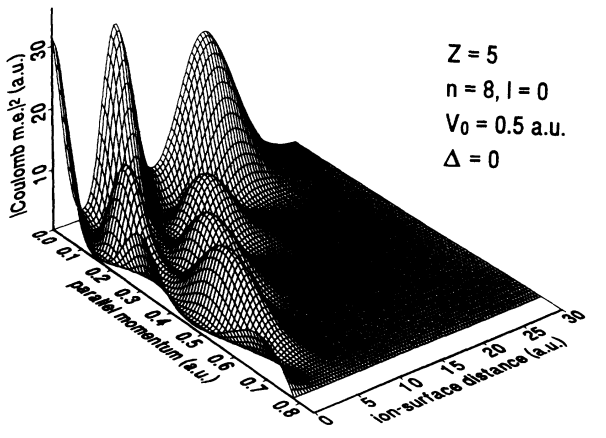

FIG. 11. Square modulus of the Coulomb matrix element for $Z=5$, $n=8$, $l=0$, $V_0=0.5$ a.u., $\Delta=0$, plotted as a function of the ion-surface distance D and the momentum component $k_{\parallel}$ of the conduction-band electron.

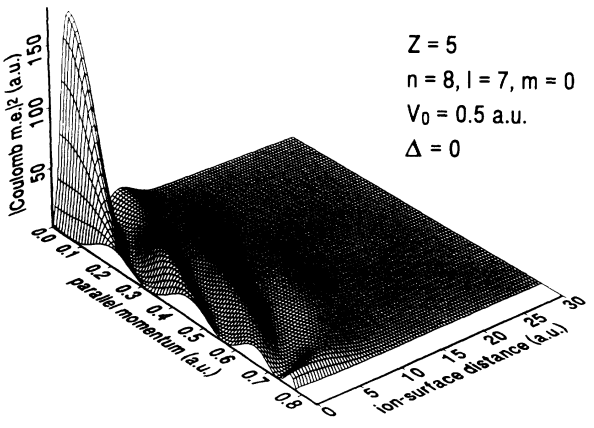

FIG. 12. Same as Fig. 11, for $l=7$, $m=0$.

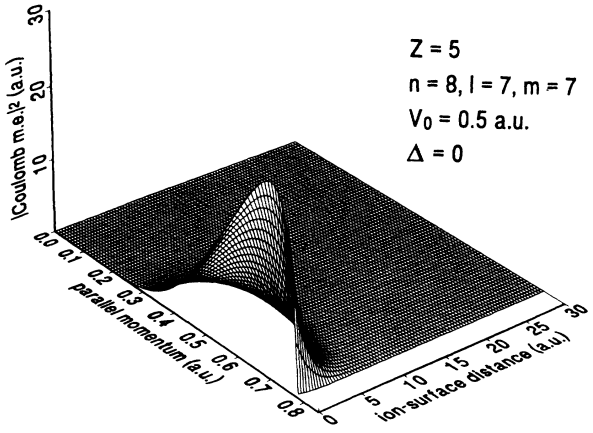

FIG. 13. Same as Fig. 11, for $l=7$, $m=7$.

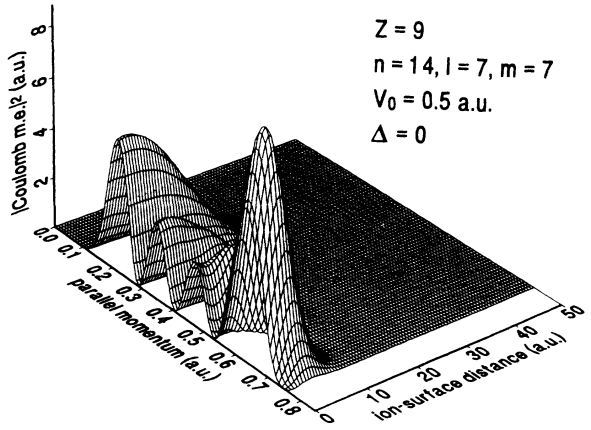

FIG. 15. Same as Fig. 14, for $l=7$, $m=7$.

only to reveal specific details of the matrix elements, but also to demonstrate that our method provides accurate results even for high-lying Rydberg states which play an important role in present-day experiments on ion–metal-surface scattering using highly charged ions [19,59]. As the energy of the $Z=9$, $n=14$ level is close to that of the $Z=5$, $n=8$ level, the $k_{\parallel}$ range covered in Fig. 14 is almost the same as that covered in Fig. 11.

The $l=0$ results shown in Fig. 14 bear qualitative similarities to those shown in Fig. 11, but exhibit a larger number of maxima. This feature can be ascribed to the larger number of radial nodes in the $n=14$, $l=0$ wave function. Incidentally, in going from Fig. 11 to Fig. 14, the number of maxima is seen to increase by about a factor of 2. This change is close to the relative change in the number of radial nodes in the corresponding wave functions. Figure 15 shows the matrix elements for the case $l=7$, $m=7$, i.e., for an l-value half in between the minimum and maximum possible values and for the maximum associated m value. The results exhibit the tendency indicated by Figs. 12 and 13, viz., the increasing localization of the matrix elements in the small-D range when l increases, and a shift towards larger $k_{\parallel}$ values when m increases. For $l=m=13$ (not shown graphically), a single spikelike structure located close to the maximum $k_{\parallel}$ value and to $D=0$ emerges.

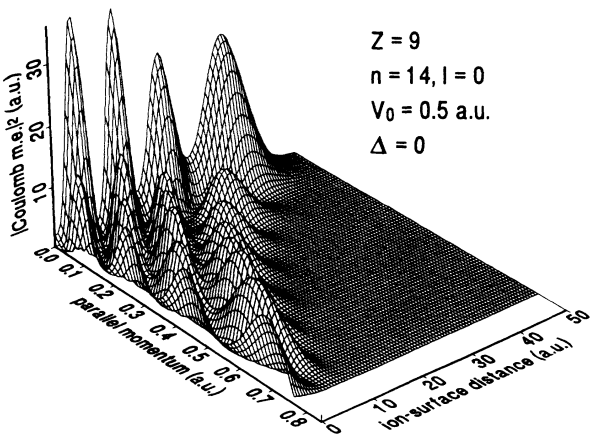

FIG. 14. Square modulus of the Coulomb matrix element for $Z=9$, $n=14$, $l=0$, $V_0=0.5$ a.u., $\Delta=0$, plotted as a function of the ion-surface distance D and the momentum component $k_{\parallel}$ of the conduction-band electron.

C. The case $\Delta\neq 0$

We now consider briefly the case of a nonzero energy defect between the conduction-band state and ionic state. The momentum components k_z and $k_{\parallel}$ are then related, in generalization of Eq. (104), by

$$k_z=[2(V_0+\Delta+\varepsilon_n)-k_{\parallel}^2]^{1/2} . \tag{105}$$

For fixed V_0 and ε_n, the maximum values for k_z and $k_{\parallel}$ are thus lowered, in comparison with the $\Delta=0$ case, when Δ is negative, and increased when Δ is positive. The physically allowed values for Δ are restricted to the range

$$|\varepsilon_n|-V_0\leq\Delta\leq|\varepsilon_n| \tag{106}$$

(we have included here the case $\Delta=|\varepsilon_n|$, i.e., $\varepsilon_k=0$, since the matrix elements $\mathcal{M}_j$ are well defined in this case and equal to $\lim_{\varepsilon_k\to 0}\mathcal{M}_j$).

In Fig. 16 the D and $k_{\parallel}$ dependence of the Coulomb matrix elements for $Z=5$, $n=8$, $l=0$, $V_0=0.5$ a.u., $\Delta=-0.2$ a.u. are shown over the full range of allowed $k_{\parallel}$ values. In comparison with the $\Delta=0$ case of Fig. 11, a smaller number of maxima emerges. This feature can be attributed to smaller k_z values and the associated larger wavelengths of the jellium wave functions inside the metal. Just the opposite tendency becomes apparent from Fig. 17, in which the case $\Delta=0.15$ a.u. is displayed.

The dependence of the Coulomb matrix elements on the energy defect Δ is shown in Figs. 18 and 19 for $D=10$ a.u. and $D=20$ a.u., respectively, for $Z=5$, $n=8$, $l=0$, $V=0.5$ a.u., $k_{\parallel}=0$. As $k_{\parallel}$ is kept fixed, the variation of Δ within the limits given by Eq. (106) implies, owing to Eq. (105), a variation of k_z within the range

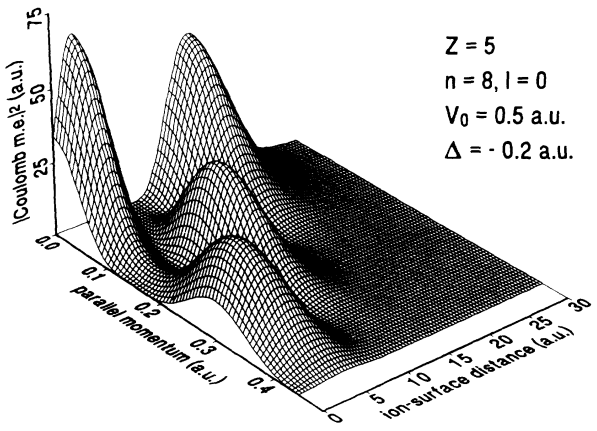

FIG. 16. Square modulus of the Coulomb matrix element for $Z=5$, $n=8$, $l=0$, $V_0=0.5$ a.u., $\Delta=-0.2$ a.u., plotted as a function of the ion-surface distance D and the momentum component $k_{\parallel}$ of the conduction-band electron.

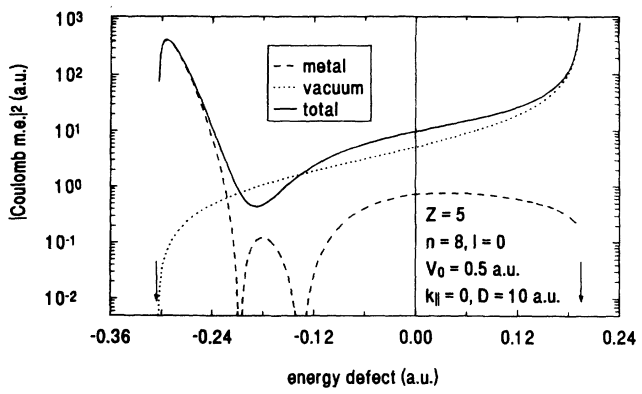

FIG. 18. Square modulus of metal contribution, vacuum contribution, and total Coulomb matrix element for $Z=5$, $n=8$, $l=0$, $V_0=0.5$ a.u., $k_{\parallel}=0$, $D=10$ a.u., plotted as a function of the energy defect Δ. The arrows delimit the range of allowed Δ values.

$0\le k_z\le(2V_0)^{1/2}$. In the immediate vicinity of $\Delta=0$, the vacuum contributions shown in Figs. 18 and 19 have been obtained by interpolation between their values at $\Delta=0$ and at suitable nonzero Δ values, at which the expression (89) could be evaluated with sufficient accuracy.

The vacuum contribution in both Figs. 18 and 19 is seen to rise monotonically from zero to its maximum value when Δ varies between its minimum and maximum value. This feature is obviously related to the exponential falloff of the jellium wave function outside of the metal. From Eqs. (14) and (105), it follows that the parameter κ_z characterizing this falloff can be expressed in terms of Δ as

$$\kappa_z=[2(|\varepsilon_n|-\Delta)]^{1/2}\ . \tag{107}$$

When Δ increases, κ_z decreases monotonically, thereby giving rise to a monotonically increasing overlap of jellium wave function and ionic wave function. The vanishing of the vacuum contribution at the lower limit $\Delta=|\varepsilon_n|-V_0$, i.e., $k_z=0$, follows immediately from the vanishing of the penetration coefficient b. At $\Delta=|\varepsilon_n|$, i.e., $\kappa_z=0$, the vacuum contribution to the matrix element itself (*not* to the square modulus) acquires a finite value given, apart from a factor of 2 arising from the penetration coefficient, by the integral of the function $f_2(\mathbf{r}-D\hat{\mathbf{e}}_z)$ over the half space $z\ge 0$. In the limiting case $D=0$, this integral can be evaluated analytically. Therefore, by numerically evaluating the vacuum contribution for the case $\Delta=|\varepsilon_n|$, $D=0$, one obtains a stringent test of the numerical procedure, in particular with regard to the overall normalization of the matrix elements.

The vanishing of the metal contribution in Figs. 18 and 19 at the lower limit $\Delta=|\varepsilon_n|-V_0$ reflects the fact that the jellium wave function vanishes inside the metal in the limit $k_z\to 0$ (note that $a\to -1$ in this limit). With increasing Δ, the metal contribution rises sharply and displays a maximum which is particularly pronounced for $D=10$ a.u. While in the latter case further structure is observed, the metal contribution for $D=20$ a.u. drops monotonically when Δ increases. At the upper limit of the allowed Δ range, the metal contribution acquires a nonzero value, which is much smaller than that of the

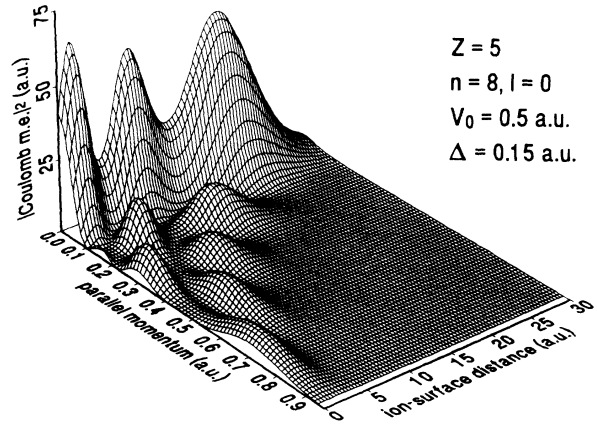

FIG. 17. Same as Fig. 16, for $\Delta=0.15$ a.u.

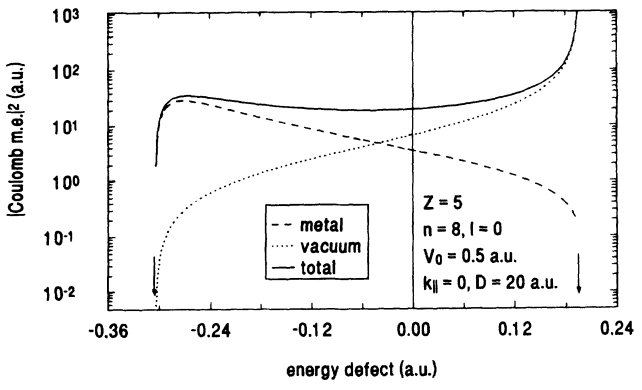

FIG. 19. Same as Fig. 18, for $D=20$ a.u.

vacuum contribution. The latter finding can be attributed to the drastically different structure of the z-dependent part of the jellium wave function inside and outside of the metal. While this part is constant outside of the metal, it exhibits rapid oscillations within the metal since k_z attains its maximum value at the upper limit of the allowed Δ range. These oscillations are likely to cause strong destructive interference in the overlap of ionic and jellium wave function.

Summarizing the discussion of Figs. 18 and 19, we conclude that the behavior of the matrix elements in the vicinity of the lower limit of the allowed Δ range is governed by the metal contribution, while at the upper limit the vacuum contribution dominates.

VI. CONCLUSIONS

We have presented in this paper a systematic evaluation of one-electron overlap and Coulomb matrix elements that appear in the theory of charge-exchange processes in ion–metal-surface scattering. By employing jellium wave functions to describe the conduction-band states of the metal and hydrogenic wave functions to describe the ionic states, the matrix elements have been evaluated in closed form for arbitrary values of their parameters. The resulting expressions for the matrix elements have been analyzed with respect to their general properties as well as to their practical computation, which requires multiple summations to be carried out numerically. It has been shown that, by appropriately arranging the various terms, the matrix elements can be computed over an enormous range of parameters.

In order to reveal finer details in the structure of the matrix elements, explicit calculations have been performed for a number of typical cases. By choosing examples pertaining to ionic Rydberg states, we have emphasized the necessity to extend the previously developed theoretical schemes into this regime and have been able to demonstrate the potentialities of our method. From the results of our calculations, detailed quantitative and qualitative information has been obtained with regard to the dependence of the matrix elements on the ion-surface distance in both the classically allowed and the classically forbidden region, on the electronic momentum in the conduction band and the ionic angular-momentum quantum numbers, and on the energy defect between conduction-band state and ionic state.

A number of applications of our method can be envisaged. The most immediate application is in the theory of charge-transfer processes in the scattering of *slow,* heavy ions by metal surfaces [59]. In the strictly adiabatic approximation, which is adequate to describe these processes, the transition rates involve only resonant matrix elements. An extension of the adiabatic picture to the truly dynamical case, in which nonresonant matrix elements are of equal importance, is clearly challenging and will provide a broad class of applications for our method. An interesting application may be brought about by the suggestion [60] to study the ion-surface interaction, in particular its dependence on the atomic angular-momentum quantum numbers l and m, by means of the scattering of state-selected Rydberg atoms. Another application involving highly excited states of neutral atoms or of ions in low charge states can possibly be found in the analysis of light emission from atoms or ions sputtered from metal surfaces [61]. Apart from applications in the field of scattering, other applications of our method may be envisaged in the study of structural properties (level broadening, level shift) of atoms adsorbed on metal surfaces. A speculative question is whether our method will be of any use in the theoretical treatment of resonant-tunneling processes of the kind occurring in scanning tunneling microscopy [62,63]. In conclusion, we believe that the method developed in this paper will be useful for discussing general properties of the ion–metal-surface interaction as well as for investigating specific static and dynamical aspects of this interaction.

ACKNOWLEDGMENTS

During the course of this work, I have benefitted from discussions with J. Burgdörfer, R. Hippler, E. Kupfer, H. O. Lutz, H. Winter (Münster), and R. Zimny.

APPENDIX A: MOMENTUM-SPACE REPRESENTATION OF $f_j(\mathbf{r})$

We define the Fourier transform ("momentum-space representation") $\tilde{f}(\mathbf{q})$ of an arbitrary function $f(\mathbf{r})$ as

$$\tilde{f}(\mathbf{q})=(2\pi)^{-3/2}\int d\mathbf{r}\exp(-i\mathbf{q}\cdot\mathbf{r})f(\mathbf{r}) . \tag{A1}$$

The inverse transform is then given by

$$f(\mathbf{r})=(2\pi)^{-3/2}\int d\mathbf{q}\exp(i\mathbf{q}\cdot\mathbf{r})\tilde{f}(\mathbf{q}) . \tag{A2}$$

The momentum-space representations $\tilde{f}_1(\mathbf{q})$ and $\tilde{f}_2(\mathbf{q})$ of the functions $f_1(\mathbf{r})$ and $f_2(\mathbf{r})$ given by Eqs. (7) and (8) are related [64] by

$$\tilde{f}_2(\mathbf{q})=-\tfrac{1}{2}(q^2+\kappa_n^2)\tilde{f}_1(\mathbf{q}) , \tag{A3}$$

where $q=|\mathbf{q}|$, and κ_n is defined by Eq. (42). It is therefore sufficient to consider explicitly the function

$$\tilde{f}_1(\mathbf{q})\equiv\tilde{\psi}_{nlm}^{(Z)}(\mathbf{q}) , \tag{A4}$$

i.e., the momentum-space representation of the normalized hydrogenic coordinate space wave function $\psi_{nlm}^{(Z)}(\mathbf{r})$. The explicit form of $\tilde{\psi}_{nlm}^{(Z)}(\mathbf{q})$ reads [65,64]

$$\tilde{\psi}_{nlm}^{(Z)}(\mathbf{q})=(-i)^l\tilde{R}_{nl}^{(Z)}(q)Y_l^m(\theta_q,\phi_q) \tag{A5}$$

[note that the factor $(-i)^l$ which obviously must be present in $\tilde{\psi}_{nlm}^{(Z)}(\mathbf{q})$ is missing in Ref. [65]], where

$$\cos\theta_q=q_z/q \tag{A6}$$

and

$$\tan\phi_q=q_y/q_x . \tag{A7}$$

The radial momentum-space wave function $\tilde{R}_{nl}^{(Z)}(q)$ is given by

$$\tilde{R}_{nl}^{(Z)}(q)=N_{nl}\frac{q^l}{(q^2+\kappa_n^2)^{l+2}}C_{n-l-1}^{l+1}\left[\frac{q^2-\kappa_n^2}{q^2+\kappa_n^2}\right] , \tag{A8}$$

where

$$N_{nl}=\left[\frac{2}{\pi}\frac{n(n-l-1)!}{(n+l)!}\right]^{1/2}2^{2(l+1)}l!\kappa_n^{l+5/2}. \tag{A9}$$

The function $C_{n-l-1}^{l+1}(x)$ is a Gegenbauer polynomial [66] given explicitly by

$$C_{n-l-1}^{l+1}(x)=\frac{1}{l!}\sum_{\nu=0}^{\nu_{\max}}(-1)^{\nu}\frac{(n-\nu-1)!}{\nu!(n-l-1-2\nu)!}\times(2x)^{n-l-1-2\nu}, \tag{A10}$$

with

$$\nu_{\max}=\left[\frac{n-l-1}{2}\right], \tag{A11}$$

where $[x]$ is the largest integer smaller than or equal to x.

Assuming the phase convention of Ref. [67], the normalized spherical harmonic $Y_l^m(\theta_q,\phi_q)$ in Eq. (A5) is given explicitly by

$$Y_l^m(\theta_q,\phi_q)=\tilde{N}_{lm}P_l^m(\cos\theta_q)\exp(im\phi_q) \tag{A12}$$

for $m\geq 0$, and

$$Y_l^{-m}(\theta_q,\phi_q)=(-1)^m Y_l^{m*}(\theta_q,\phi_q), \tag{A13}$$

where

$$\tilde{N}_{lm}=(-1)^m\left[\frac{(2l+1)(l-m)!}{4\pi(l+m)!}\right]^{1/2}. \tag{A14}$$

The associated Legendre function $P_l^m(\cos\theta_q)$ can be expressed as

$$P_l^m(\cos\theta_q)=\frac{(-1)^l}{2^l l!}(1-\cos^2\theta_q)^{m/2}\times\sum_{\lambda=\lambda_{\min}}^{l}(-1)^{\lambda}\binom{l}{\lambda}\frac{(2\lambda)!}{(2\lambda-l-m)!}\times(\cos\theta_q)^{2\lambda-l-m}, \tag{A15}$$

where

$$\lambda_{\min}=\left[\frac{l+m+1}{2}\right]. \tag{A16}$$

APPENDIX B: EXPLICIT FORM OF $\mathcal{P}_{nl}(q_z)$ AND $\mathcal{Q}_{lm}(q_z)$

The explicit form of the polynomials $\mathcal{P}_{nl}(q_z)$ follows from Eqs. (49) and (52) as

$$\begin{aligned}\mathcal{P}_{nl}(q_z)&=N_{nl}(q_z^2+k_+'^2)^{n-l-1}C_{n-l-1}^{l+1}\left[\frac{q_z^2+k_-'^2}{q_z^2+k_+'^2}\right]\\&=\frac{N_{nl}}{l!}\sum_{\nu=0}^{\nu_{\max}}(-1)^{\nu}\frac{(n-\nu-1)!}{\nu!(n-l-1-2\nu)!}[2(q_z^2+k_-'^2)]^{n-l-1-2\nu}(q_z^2+k_+'^2)^{2\nu}\\&=\mathcal{A}(Z;n,l)\sum_{\nu=0}^{\nu_{\max}}\mathcal{B}(n,l;\nu)\sum_{\alpha=0}^{n-l-2\nu-1}\mathcal{C}(Z;n,l;\nu;\alpha;k_\parallel')\sum_{\beta=0}^{2\nu}\mathcal{D}(Z;n;\nu;\beta;k_\parallel')q_z^{2(\alpha+\beta)},\end{aligned} \tag{B1}$$

where the coefficients $\mathcal{A},\mathcal{B},\mathcal{C},\mathcal{D}$ are given by

$$\mathcal{A}(Z;n,l)=\pi^{-1/2}2^{n+l+3/2}\kappa_n^{l+5/2}\left[n(n-l)\binom{n}{l}\Big/\binom{n+l}{l}\right]^{1/2}, \tag{B2}$$

$$\mathcal{B}(n,l;\nu)=(-1)^{\nu}2^{-2\nu}\binom{n-l-1}{2\nu}\binom{2\nu}{\nu}\left[(n-\nu)\binom{n}{\nu}\right]^{-1}, \tag{B3}$$

$$\mathcal{C}(Z;n,l;\nu;\alpha;k_\parallel')=\binom{n-l-2\nu-1}{\alpha}k_-'^{2(n-l-2\nu-1-\alpha)}, \tag{B4}$$

$$\mathcal{D}(Z;n;\nu;\beta;k_\parallel')=\binom{2\nu}{\beta}k_+'^{2(2\nu-\beta)}. \tag{B5}$$

In the specific form in which these coefficients are written, they involve binomial coefficients, but no factorials. By eliminating the factorials completely, the accuracy of the numerical evaluation of the matrix elements is increased (cf. Sec. IV D).

Similarly, we obtain for the polynomials $\mathcal{Q}_{lm}(q_z)$ from Eqs. (51) and (53)

$$\begin{aligned}\mathcal{Q}_{lm}(q_z)&=\tilde{N}_{lm}(q_z^2+k_\parallel'^2)^{l/2}P_l^m\left[\frac{q_z}{(q_z^2+k_\parallel'^2)^{1/2}}\right]\exp(im\phi_{k'})\\&=\frac{(-1)^l\tilde{N}_{lm}}{2^l l!}k_\parallel'^m\exp(im\phi_{k'})\sum_{\lambda=\lambda_{\min}}^{l}(-1)^{\lambda}\binom{l}{\lambda}\frac{(2\lambda)!}{(2\lambda-l-m)!}q_z^{2\lambda-l-m}(q_z^2+k_\parallel'^2)^{l-\lambda}\\&=\tilde{\mathcal{A}}(l,m;k_x',k_y')\sum_{\lambda=\lambda_{\min}}^{l}\tilde{\mathcal{B}}(l,m;\lambda)\sum_{\gamma=0}^{l-\lambda}\tilde{\mathcal{C}}(l;\lambda;\gamma;k_\parallel')q_z^{2(\lambda+\gamma)-l-m},\end{aligned} \tag{B6}$$

where

$$\tilde{\mathcal{A}}(l,m;k'_x,k'_y)=(-1)^{l+m}\exp(im\phi_{k'})\pi^{-1/2}2^{-l-1}k'^{m}_{\parallel}\left[(2l+1)\binom{l+m}{m}\Big/\binom{l}{m}\right]^{1/2} \text{ if } m\geq 0 , \tag{B7}$$

$$\tilde{\mathcal{A}}(l,-m;k'_x,k'_y)=(-1)^{m}\tilde{\mathcal{A}}^{*}(l,m;k'_x,k'_y) , \tag{B8}$$

$$\tilde{\mathcal{B}}(l,m;\lambda)=(-1)^{\lambda}\binom{l}{\lambda}\binom{2\lambda}{l+m} , \tag{B9}$$

$$\tilde{\mathcal{C}}(l;\lambda;\gamma;k'_{\parallel})=\binom{l-\lambda}{\gamma}k'^{2(l-\lambda-\gamma)}_{\parallel} . \tag{B10}$$

The explicit form of the polynomials $\mathcal{F}_j(q_z)$ follows by inserting Eqs. (B1) and (B6) into Eq. (59).

APPENDIX C: EXPLICIT FORM OF $\mathcal{V}^{(v)}_{nl}(k'_+)$ and $\mathcal{W}^{(w)}_{lm}(k'_+)$

Using Eq. (B1) and (B6), it follows from the definitions (80) and (81) that

$$\mathcal{V}^{(v)}_{nl}(k'_+)=(-1)^{v}\mathcal{A}(Z;n,l)\sum_{\nu=0}^{\nu_{\max}}k'^{4\nu}_{+}\mathcal{B}(n,l;\nu)\sum_{\alpha=0}^{n-l-2\nu-1}(-1)^{\alpha}k'^{2\alpha}_{+}\mathcal{C}(Z;n,l;\nu;\alpha;k'_{\parallel})\sum_{\beta=0}^{2\nu}\mathcal{E}^{(v)}(\nu;\alpha,\beta) , \tag{C1}$$

where

$$\mathcal{E}^{(v)}(\nu;\alpha,\beta)=(-1)^{\beta}\binom{2\nu}{\beta}\binom{2(\alpha+\beta)}{v}\Theta(2(\alpha+\beta)-v) , \tag{C2}$$

and

$$\mathcal{W}^{(w)}_{lm}(k'_+)=(-1)^{w}i^{l+m}\tilde{\mathcal{A}}(l,m;k'_x,k'_y)\sum_{\lambda=\lambda_{\min}}^{l}(-1)^{\lambda}k'^{2\lambda-l-m}_{+}\tilde{\mathcal{B}}(l,m;\lambda)\sum_{\gamma=0}^{l-\lambda}\tilde{\mathcal{E}}^{(w)}(Z;n,l,m;\lambda;\gamma;k'_{\parallel}) , \tag{C3}$$

where

$$\tilde{\mathcal{E}}^{(w)}(Z;n,l,m;\lambda;\gamma;k'_{\parallel})=(-1)^{\gamma}\binom{l-\lambda}{\gamma}\binom{2(\lambda+\gamma)-l-m}{w}k'^{2(l-\lambda-\gamma)}_{\parallel}k'^{2\gamma}_{+}\Theta(2(\lambda+\gamma)-l-m-w) . \tag{C4}$$

The function $\Theta(\ )$ introduced in Eqs. (C2) and (C4) is the unit step function, with the proviso $\Theta(0)=1$.

Note that in the final expression (84) for the matrix elements $\mathcal{M}_j$ a phase factor $(-i)^{l+m}\exp(im\phi_{k'})$ is assumed to be removed from the expression (C3) for the function $\mathcal{W}^{(w)}_{lm}(k'_+)$ and is incorporated into an overall phase factor of the matrix elements.

[1] M. L. E. Oliphant and P. B. Moon, Proc. R. Soc. (London) Ser. A **127**, 404 (1930).

[2] H. S. W. Massey, Proc. Cambridge Philos. Soc. **26**, 386 (1930); **27**, 460 (1931).

[3] S. S. Shekhter, Zh. Eksp. Teor. Fiz. **7**, 750 (1937).

[4] A. Cobas and W. E. Lamb, Phys. Rev. **65**, 327 (1944).

[5] H. D. Hagstrum, Phys. Rev. **89**, 244 (1953); **91**, 543 (1953); **96**, 325 (1954); **96**, 336 (1954).

[6] H. D. Hagstrum, in *Inelastic Ion-Surface Collisions,* edited by N. H. Tolk, J. C. Tully, W. Heiland, and C. W. White (Academic, New York, 1977), p. 1.

[7] H. D. Hagstrum, in *Electron and Ion Spectroscopy of Solids,* edited by L. Fiermans, J. Vennik, and W. Dekeyser (Plenum, New York, 1978), p. 273.

[8] D. M. Newns, K. Makoshi, R. Brako, and J. N. M. van Wunnik, Phys. Scr. **T6**, 5 (1983).

[9] J. N. M. van Wunnik and J. Los, Phys. Scr. **T6**, 27 (1983).

[10] P. Varga, Appl. Phys. A **44**, 31 (1987).

[11] H. J. Andrä, in *Fundamental Processes of Atomic Dynamics,* edited by J. S. Briggs, H. Kleinpoppen, and H. O. Lutz (Plenum, New York, 1988), p. 631.

[12] H. Winter and R. Zimny, in *Coherence in Atomic Collision Physics,* edited by H. J. Beyer, K. Blum, and R. Hippler (Plenum, New York, 1988), p. 283.

[13] R. Brako and D. M. Newns, in *Proceedings of the Fifteenth International Conference on the Physics of Electronic and Atomic Collisions, Brighton, 1987,* edited by H. B. Gilbody, W. R. Newell, F. H. Read, and A. C. H. Smith (North-Holland, Amsterdam, 1988), p. 783.

[14] P. Varga, in Ref. [13], p. 793.

[15] H. Winter and R. Zimny, in Ref. [13], p. 811.

[16] R. Brako and D. M. Newns, Rep. Prog. Phys. **52**, 655 (1989).

[17] P. Varga, Comments At. Mol. Phys. **23**, 111 (1989).

[18] H. J. Andrä, Nucl. Instrum. Methods **43**, 306 (1989).

[19] H. J. Andrä, in *Physics of Highly Ionized Atoms,* edited by R. Marrus (Plenum, New York, 1989), p. 377.

[20] J. Los and J. J. C. Geerlings, Phys. Rep. **190**, 133 (1990).

[21] H. Winter, Comments At. Mol. Phys. **26**, 287 (1991).

[22] J. W. Gadzuk, Surf. Sci. **6**, 133 (1967); **6**, 159 (1967).

[23] B. A. Trubnikov and Yu. N. Yavlinskii, Zh. Eksp. Teor. Fiz. **52**, 1638 (1967) [Sov. Phys.—JETP **25**, 1089 (1967)].

[24] M. Remy, J. Chem. Phys. **53**, 2487 (1970).

[25] U. A. Arifov, L. M. Kishinevskii, E. S. Mukhamadiev, and E. S. Parilis, Zh. Tekh. Fiz. **43**, 181 (1973) [Sov. Phys.—Tech. Phys. **18**, 118 (1973)].

[26] R. Hentschke, K. J. Snowdon, P. Hertel, and W. Heiland, Surf. Sci. **173**, 565 (1986).

[27] K. J. Snowdon, R. Hentschke, A. Närmann, and W. Heiland, Surf. Sci. **173**, 581 (1986).
[28] S. T. de Zwart, Ph. D. thesis, Rijksuniversiteit Groningen, 1987 (unpublished).
[29] R. Zimny, H. Nienhaus, and H. Winter, Radiat. Eff. Defects Solids **109**, 9 (1989).
[30] A. V. Chaplik, Zh. Eksp. Teor. Fiz. **54**, 332 (1968) [Sov. Phys.—JETP **27**, 178 (1968)].
[31] R. K. Janev, J. Phys. B **7**, 1506 (1974).
[32] R. K. Janev and N. N. Nedeljkovic, J. Phys. B **14**, 2995 (1981); **18**, 915 (1985).
[33] N. N. Nedeljkovic, R. K. Janev, and V. Yu. Lazur, Phys. Rev. B **38**, 3088 (1988).
[34] P. Nordlander and J. C. Tully, in *Proceedings of the Sixteenth International Conference on the Physics of Electronic and Atomic Collisions, New York, 1989,* edited by A. Dalgarno, R. S. Freund, P. M. Koch, M. S. Lubell, and T. B. Lucatorto (AIP, New York, 1990), p. 529.
[35] P. Nordlander and J. C. Tully, Phys. Rev. B **42**, 5564 (1990).
[36] A. Blandin, A. Nourtier, and D. W. Hone, J. Phys. (Paris) **37**, 369 (1976).
[37] H. Schröder and E. Kupfer, Z. Phys. A **279**, 13 (1976).
[38] J. C. Tully, Phys. Rev. B **10**, 4324 (1977).
[39] W. Bloss and D. Hone, Surf. Sci. **72**, 277 (1978).
[40] R. Brako and D. M. Newns, Surf. Sci. **108**, 253 (1981).
[41] E. Kupfer and H. Schröder, Z. Phys. A **315**, 35 (1984).
[42] J. Burgdörfer and E. Kupfer, Phys. Rev. Lett. **57**, 2649 (1986).
[43] J. Burgdörfer, E. Kupfer, and H. Gabriel, Phys. Rev. A **36**, 4963 (1987).
[44] U. Thumm and J. S. Briggs, Nucl. Instrum. Methods B **43**, 471 (1989).
[45] U. Thumm, Ph.D. thesis, Universität Freiburg, 1989 (unpublished).
[46] E. G. Overbosch, B. Rasser, A. D. Tenner, and J. Los, Surf. Sci. **92**, 310 (1980).
[47] Proceedings of the Conference on the Physics of Multiply Charged Ions, Groningen, 1986, edited by R. Morgenstern, A. Niehaus, F. J. de Heer, and A. G. Drentje [Nucl. Instrum. Methods B **23**, Nos. 1 and 2 (1987)].
[48] Proceedings of the International Conference on the Physics of Multiply Charged Ions and International Workshop on E. C. R. Ion Sources, Grenoble, 1988, edited by S. Bliman [J. Phys. (Paris) **50**, C1 (1989)].
[49] J. P. Briand, L. de Billy, P. Charles, S. Essabaa, P. Briand, R. Geller, J. P. Desclaux, S. Bliman, and C. Ristori, Phys. Rev. Lett. **65**, 159 (1990).
[50] L. Folkerts and R. Morgenstern, Europhys. Lett. **13**, 377 (1990).
[51] Proceedings of the Vth International Conference on the Physics of Multiply Charged Ions, Giessen, 1990, edited by E. Salzborn, P. H. Mokler, and A. Müller [Z. Phys. D **21**, Suppl. (1991)].
[52] R. Köhrbrück, D. Lecler, F. Fremont, P. Roncin, K. Sommer, T. J. M. Zouros, J. Bleck-Neuhaus, and N. Stolterfoht, Nucl. Instrum. Methods B **56/57**, 219 (1991).
[53] M. Schulz, C. L. Cocke, S. Hagmann, M. Stöckli, and H. Schmidt-Böcking, Phys. Rev. A **44**, 1653 (1991).
[54] J. Burgdörfer, P. Lerner, and F. W. Meyer, Phys. Rev. A **44**, 5674 (1991).
[55] J. N. Bardsley and B. M. Penetrante (unpublished).
[56] E. Kupfer (private communication).
[57] M. R. C. McDowell and J. P. Coleman, *Introduction to the Theory of Ion-Atom Collisions* (North-Holland, Amsterdam, 1970).
[58] P. M. Morse and H. Feshbach, *Methods of Theoretical Physics* (McGraw-Hill, New York, 1953), Pt. I, Chap. 4.5.
[59] U. Wille, Nucl. Instrum. Methods (to be published).
[60] H. O. Lutz (private communication).
[61] S. Reinke, D. Rahmann, and R. Hippler, Vacuum **42**, 807 (1991).
[62] J. Tersoff and D. R. Hamann, Phys. Rev. B **31**, 805 (1985).
[63] T. E. Feuchtwang and P. H. Cutler, Phys. Scr. **38**, 252 (1988).
[64] R. M. May, Phys. Rev. **136**, A669 (1964).
[65] H. A. Bethe and E. E. Salpeter, in *Handbuch der Physik,* edited by S. Flügge (Springer, Berlin, 1957), Vol. XXXV, p. 88.
[66] *Handbook of Mathematical Functions,* edited by M. Abramowitz and I. A. Stegun (Dover, New York, 1965), Chap. 22.3.
[67] A. R. Edmonds, *Angular Momentum in Quantum Mechanics* (Princeton University Press, Princeton, 1960).

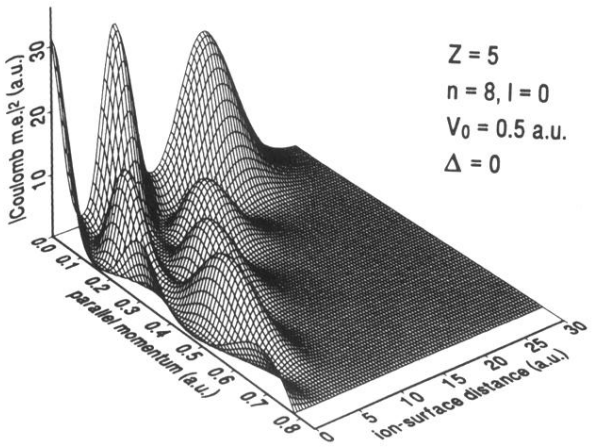

FIG. 11. Square modulus of the Coulomb matrix element for $Z=5$, $n=8$, $l=0$, $V_0=0.5$ a.u., $\Delta=0$, plotted as a function of the ion-surface distance D and the momentum component $k_{\parallel}$ of the conduction-band electron.

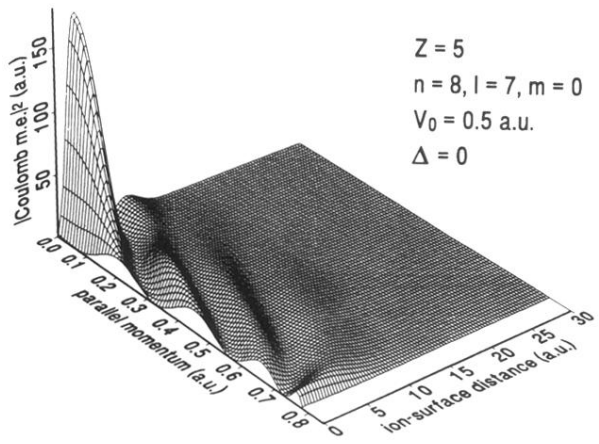

FIG. 12. Same as Fig. 11, for $l=7$, $m=0$.

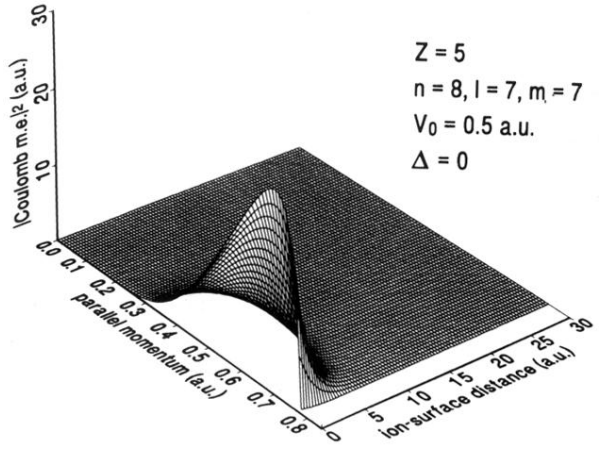

FIG. 13. Same as Fig. 11, for $l=7$, $m=7$.

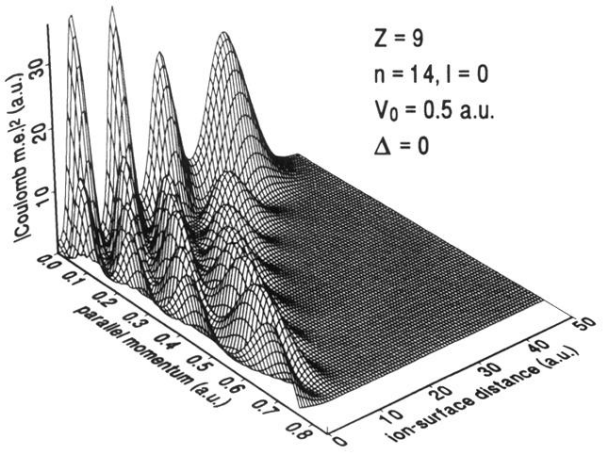

FIG. 14. Square modulus of the Coulomb matrix element for $Z=9$, $n=14$, $l=0$, $V_0=0.5$ a.u., $\Delta=0$, plotted as a function of the ion-surface distance D and the momentum component $k_{\parallel}$ of the conduction-band electron.

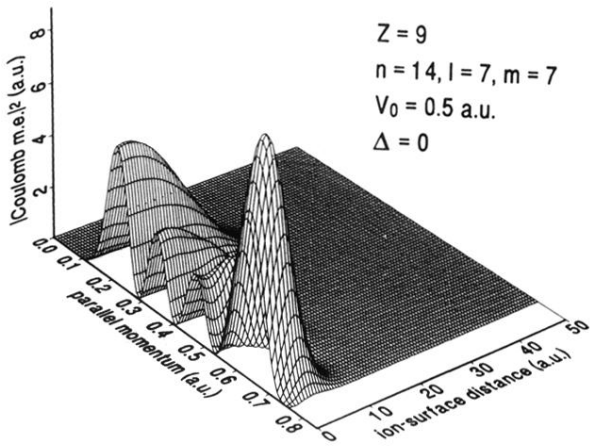

FIG. 15. Same as Fig. 14, for $l=7$, $m=7$.

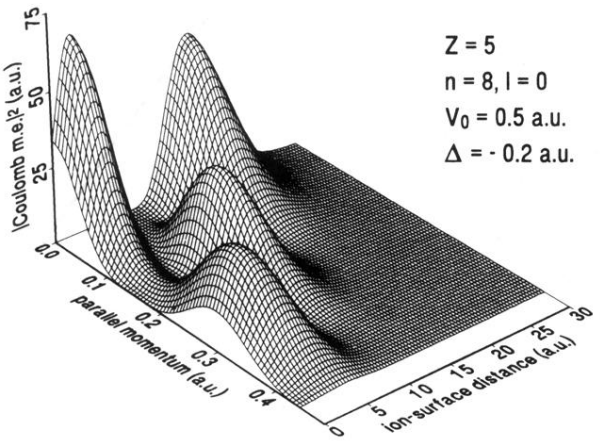

FIG. 16. Square modulus of the Coulomb matrix element for $Z=5$, $n=8$, $l=0$, $V_0=0.5$ a.u., $\Delta=-0.2$ a.u., plotted as a function of the ion-surface distance D and the momentum component $k_{\parallel}$ of the conduction-band electron.

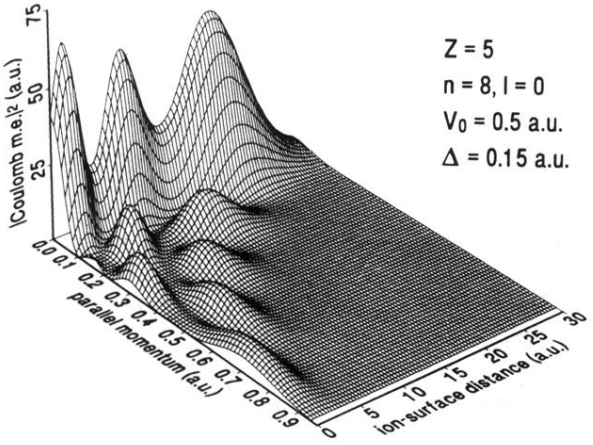

FIG. 17. Same as Fig. 16, for $\Delta = 0.15$ a.u.